JACS
JOURNAL OF THE AMERICAN CHEMICAL SOCIETY
Article
pubs.acs.org/JACS

# Two-State Reactivity in Low-Valent Iron-Mediated C−H Activation and the Implications for Other First-Row Transition Metals

Yihua Sun,[†] Hao Tang,[†] Kejuan Chen,[†] Lianrui Hu,[†] Jiannian Yao,[†] Sason Shaik,[‡] and Hui Chen*[,†]

[†]Beijing National Laboratory for Molecular Sciences (BNLMS), Key Laboratory of Photochemistry, Institute of Chemistry, Chinese Academy of Sciences, Beijing 100190, P. R. China

[‡]Institute of Chemistry and the Lise Meitner-Minerva Center for Computational Quantum Chemistry, The Hebrew University of Jerusalem, 91904 Jerusalem, Israel

Supporting Information

**ABSTRACT:** C−H bond activation/functionalization promoted by low-valent iron complexes has recently emerged as a promising approach for the utilization of earth-abundant first-row transition metals to carry out this difficult transformation. Herein we use extensive density functional theory and high-level ab initio coupled cluster calculations to shed light on the mechanism of these intriguing reactions. *Our key mechanistic discovery for C−H arylation reactions reveals a two-state reactivity (TSR) scenario in which the low-spin Fe(II) singlet state, which is initially an excited state, crosses over the high-spin ground state and promotes C−H bond cleavage.* Subsequently, aryl transmetalation occurs, followed by oxidation of Fe(II) to Fe(III) in a single-electron transfer (SET) step in which dichloroalkane serves as an oxidant, thus promoting the final C−C coupling and finalizing the C−H functionalization. Regeneration of the Fe(II) catalyst for the next round of C−H activation involves SET oxidation of the Fe(I) species generated after the C−C bond coupling. *The ligand sphere of iron is found to play a crucial role in the TSR mechanism by stabilization of the reactive low-spin state that mediates the C−H activation.* This is the first time that the successful TSR concept conceived for high-valent iron chemistry is shown to successfully rationalize the reactivity for a reaction promoted by low-valent iron complexes. A comparative study involving other divalent middle and late first-row transition metals implicates iron as the optimum metal in this TSR mechanism for C−H activation. It is predicted that stabilization of low-spin Mn(II) using an appropriate ligand sphere should produce another promising candidate for efficient C−H bond activation. This new TSR scenario therefore emerges as a new strategy for using low-valent first-row transition metals for C−H activation reactions.

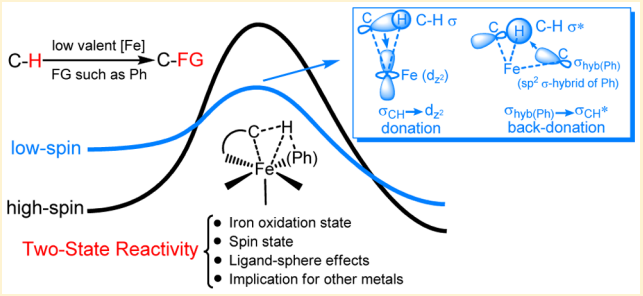


## 1. INTRODUCTION

Bioorganisms use mostly middle and late first-row transition metals (TMs), i.e., Mn, Fe, Co, Ni, and Cu, to carry out key biochemical reactions, including the activation and functionalization of strong C−H bonds.[1−6] In contrast, in homogeneous catalysis these earth-abundant and cheaper first-row TMs are still less exploited for C−H activation/functionalization compared with second- and third-row noble TMs such as Ru, Rh, Pd, and Pt.[7] Among the first-row TMs, iron has received special attention because of its large abundance in the earth's crust, its rich chemistry from a variety of oxidation states, and its wide occurrence in biological metalloenzymes.[2,8]

Sporadic examples of stoichiometric C−H bond activation/functionalization mediated by low-valent iron (hereafter, oxidation state below III) have been known for decades.[9−12] However, a renaissance in harnessing low-valent iron complexes to perform efficient C−H activation/functionalization in homogeneous catalysis (see Scheme 1) has transpired only recently. Experimentally, a notable breakthrough is the report about the iron-catalyzed direct arylation reaction via directed $sp^2$ C−H bond activation by Nakamura and co-workers in 2008.[13] In this iron-catalyzed $sp^2$ C−H bond activation reaction (Scheme 1a), a *N,N*-bidentate ligand, e.g., bipyridine or 1,10-phenanthroline (phen), is required to effect the transformation, but the reasons for this are still unclear. Although requiring a very intricate control of reaction conditions, this reaction can be carried out at mild temperatures (0 °C) and exhibits versatile reactivity toward substrates having a variety of functional groups. Following the above pioneering study, iron-catalyzed C−H activation/functionalization was successfully extended by Nakamura, Cook, Ackermann, DeBoef, and their co-workers to include a variety of chemical transformations involving, inter alia, allylation, alkylation, and amination besides arylation,[14−18] different types of $sp^2$ C−H bonds (alkenyl $sp^2$ C−H bonds besides aryl ones),[15,19,20] various directing groups for C−H bond activation,[21−24] and even more inert $sp^3$ C−H bond activations.[25−28] Interestingly, for many of these recently developed reactions, including the activation of inert $sp^3$ C−H bonds,[14−18,20,25,26] diphosphine-

**Received:** November 19, 2015
**Published:** February 23, 2016





DOI: 10.1021/jacs.5b12150
J. Am. Chem. Soc. 2016, 138, 3715−3730

**Scheme 1. Selected Examples of Recent Advances in Low-Valent Fe-Catalyzed C−H Activation/Functionalization Reactions; The Ligand Spheres Are Shown in the Boxes**

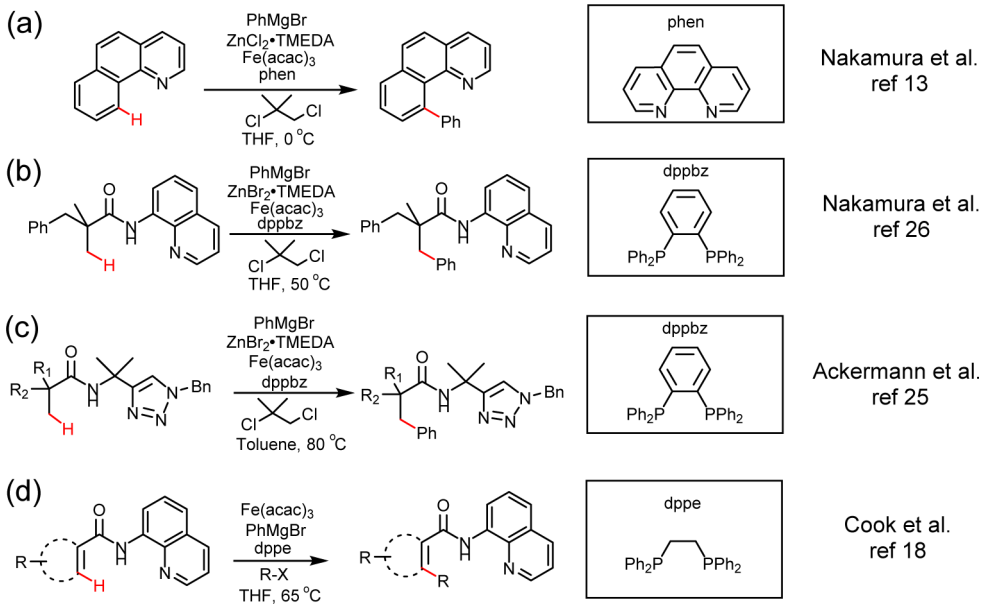


type ligands (see Scheme 1) were found to be superior to the previously used *N*,*N*-bidentate bipyridine ligands.[13] The reason for the superiority of these newly used ligands is also still unclear. As such, despite the considerable experimental advances in these low-valent iron catalyses, many mechanistic issues remain unclear, such as the role played by the ligand sphere. What is needed to address these issues is to establish a clear mechanism for these transformations, thereby contributing insight that will enable one to optimize this way of C−H activation/functionalization. This is the goal in the present paper.

Nature utilizes high-valent iron(IV)−oxo species to bring about many C−H activation processes, mainly via a radical mechanism that is initiated by H atom abstraction.[2a−c,k,29] To this end, the concepts of two-state reactivity (TSR) and multistate reactivity (MSR) have been proposed by some of us to describe the mechanistic features of these reactions.[30] TSR and MSR involve more than one spin state in reactions; one or some of these states perform the C−H bond activation, while another completes the bond functionalization (e.g., to alcohol) by means of radical rebound. These concepts have contributed substantially to the understanding of the reactivity of enzymes and their synthetic mimics.[31]

Can these concepts also shed light on the mechanistic understanding of low-valent iron-mediated reactions? We think they can! After all, compared with second- and third-row TMs, which tend to favor closed-shell singlet electronic states, earth-abundant first-row TMs are more likely to involve open-shell electronic structures, which are often associated with multiple spin states close in energy and hence in principle should be subject to two-state or multistate considerations. However, in contrast to the extensively studied TSR and MSR in high-valent iron-mediated reactions, in the area of low-valent iron-mediated reactions, theoretical explorations of the involvement of multiple spin states are still quite rare and have been investigated only for a very limited number of reactions.[32] Furthermore, for organometallic reactions promoted by other low-valent middle/late first-row TMs besides Fe (i.e., Mn, Co, Ni, Cu), to date there have been only a few sporadic studies considering multiple spin states.[33] Thus, despite pioneering recognition of the importance of considering multiple spin states in TM-mediated reactions,[30,34] their intriguing role in low-valent earth-abundant first-row TMs remains largely unexplored.[35] In this work, we use extensive density functional theory (DFT) and high-level ab initio coupled cluster calculations to demonstrate that a TSR scenario operates in low-valent iron-catalyzed C−H activation and is the root cause of the ability of the complex to activate the C−H bond. Thereafter, the subsequent C−C bond formation occurs on one spin state. This extension of the TSR concept from bioinorganic reactions of high-valent iron to organometallic reactions of low-valent iron not only brings order to low-valent iron catalysis but also opens up new opportunities for modulating and controlling reactivity patterns of low-valent organometallic reactions promoted by other earth-abundant TMs, which is an appealing and fast-growing field in homogeneous catalysis. To our best knowledge, this work is the first theoretical exploration of a puzzles-laden mechanism for the recently developed low-valent iron-catalyzed C−H activation/functionalization reactions. For pursuit of insights into the wider scope of catalysis by earth-abundant TMs, we also compare the iron-promoted reaction with the corresponding hypothetical ones mediated by other low-valent middle/late first-row TMs (Mn, Co, Ni, Cu), providing new insights for future experimental and computational developments.

## 2. COMPUTATIONAL DETAILS

All of the DFT calculations were performed using the Gaussian 09 suite of programs.[36] The geometries of all minima and transition states (TSs) were fully optimized in the gas phase without any symmetry constraints using the B3LYP hybrid density functional[37] in combination with the def2-SVP basis set[38] (B1) for all of the atoms. The unrestricted formalism of B3LYP was used for open-shell calculations. Harmonic vibrational frequency calculations were performed to verify the natures of the stationary points obtained in the geometry optimizations as well as to get the thermal Gibbs free energy corrections. All of the minima were verified to have no imaginary frequencies, whereas all of the optimized TSs were confirmed to have only one proper imaginary frequency. Intrinsic


DOI: 10.1021/jacs.5b12150
J. Am. Chem. Soc. 2016, 138, 3715−3730

reaction coordinate (IRC) calculations were also conducted to ensure that all of the reported TSs properly link the corresponding minima.

The electronic energy was refined using B3LYP single-point calculations on the optimized geometries with the larger def2-TZVP basis set[38] (B2). In all of the B2 single-point calculations except those used for the comparison among middle/late TMs (Mn, Fe, Co, Ni, and Cu, calculated in the gas phase), the SMD continuum solvation model[39] was utilized to take solvent effects into consideration. The experimentally employed solvents were used for solvent effect modeling. Dispersion corrections were derived using the DFT-D3 method[40] (with the Becke–Johnson short-range damping scheme) in the B2 single-point calculations. The thermal corrections to the Gibbs free energy were calculated in the gas phase at room temperature, since all of the related reactions were done mildly at relatively low temperatures. The reported free energies in this work include the B2 electronic energy in solution (including the solvation free energy correction), the DFT-D3 energy correction, and the thermal correction to the Gibbs free energy. The semiclassical kinetic isotope effect (KIE) of the $sp^3$ C–H activation was calculated using eq 1 derived from the Eyring model,

$$\mathrm{KIE} = k_H/k_D = \exp[(\Delta G_D^{\ddagger} - \Delta G_H^{\ddagger})/RT] \quad (1)$$

in which the free energies of activation ($\Delta G^{\ddagger}$) were calculated at the reaction temperature.

To address the crucial but tough issue of spin-state energetics for iron(II) species in DFT calculations, high-level partially spin-adapted open-shell coupled cluster RCCSD(T) calibration calculations were performed with Molpro.[41] To reduce the prohibitive computational expense of coupled cluster calculations, we used truncated reaction models in the CCSD(T) calculations. The truncation from the experimental catalytic models kept unchanged the first coordinate sphere of iron. To mimic the experimental models as closely as possible, in the truncated models, we fixed the positions of all of the non-hydrogen atoms and hydrogen atoms that exist in the experimental model as in the DFT-optimized geometries of the experimental model while optimizing the positions of the newly added H atoms in the truncated model.

To address the basis set incompleteness error in valence-correlated CCSD(T) calculations, we carried out complete basis set (CBS) limit extrapolations using the correlation-consistent cc-pVDZ and cc-pVTZ basis sets[42] according to eq 2,[43] which was found recently to be superior to alternative extrapolation schemes.[44]

$$E_{\mathrm{total},n} = E_{\mathrm{total,CBS}} + \frac{A}{(n + 1/2)^4} \quad (2)$$

To properly treat the iron 3s3p outer-core–valence correlation, we also performed the 3s3p core–valence correlation effect calculations at the CCSD(T) level with the optimized core–valence correlation-weighted cc-pwCVDZ basis set for the Fe atom and the cc-pVDZ basis set for the remaining atoms (denoted as wDZ).[42] The outer-core–valence correlation correction was obtained by subtracting the energy without core–valence correlation from the one with core–valence correlation, both calculated with the same wDZ basis set. Our final reported CCSD(T) results include both the valence-correlated CCSD(T)/CBS data and the core–valence correlation correction. For these first-row TM species containing iron, which often suffer from the convergence problem of the Hartree–Fock (HF) method,[45] our CCSD(T) calculations made use of B3LYP Kohn–Sham orbitals as the reference orbitals. In our case, the self-consistent field calculations converged with both the B3LYP and HF methods only for singlet states, and their calculated barriers differed only by 0.1 kcal/mol at the valence-correlated CCSD(T)/cc-pVDZ level. This test showed that the dependence of our CCSD(T) results on orbital variations is very small. Furthermore, the values of the T1 diagnostic, often taken as a measure of multireference character, were smaller than 0.03 in all of our CCSD(T) calculations (see Table S2 in the Supporting Information). These results imply that the multireference character of the calculated species is not significant, so our CCSD(T) calculations should be reliable. To obtain the corrections for DFT calculations of the larger and more realistic experimental systems, we compared the final CCSD(T)/CBS results including the 3s3p core–valence correlation effect to those calculated from our adopted DFT level (B3LYP/B2) for the same truncated model systems, the differences of which were added as the corrections to the DFT results for the larger experimental models.

## 3. RESULTS AND DISCUSSION

**3.1. Two-State Mechanism of Low-Valent Iron-Mediated C–H Activation/Functionalization.** In almost all of the recently studied low-valent iron-catalyzed C–H activation/functionalization reactions,[13−23,25,26,28] the reactions were conducted in a very reductive environment with excess organometallic reagents such as Grignard or organozinc reagents, which minimize the presence and involvement of oxidative high-valent iron such as Fe(IV) or Fe(V) species in the reactions. Although Fe(III) salts like $FeCl_3$ and $Fe(acac)_3$ were commonly used as precatalysts in most of the iron-mediated C–H activations/functionalizations, it is unlikely that Fe(III) directly takes part in the initiation of the C–H activation step of the reaction in the reductive environment mentioned above for the following reasons: (a) the use of Fe(II) salts such as $FeCl_2$ as the precatalyst was found to be almost as effective as using Fe(III) salts;[13,16] (b) in the reductive reaction environment with Grignard or organozinc reagents, Fe(II) or lower-valent iron will be generated from relatively oxidative Fe(III);[46] and (c) it has been found experimentally that even in the absence of dichloroalkane oxidant, which is potentially capable of oxidizing lower-valent iron to Fe(III), the C–H activation step still takes place.[16]

Despite these considerations, it is important to point out that in the very recent experiments by Nakamura and co-workers utilizing less reductive organoboron or organoaluminum reagents, Fe(III) was proposed to be the active oxidation state for C–H activation.[24,27] However, there exists a key difference between the recent experiments utilizing less reductive reagents and the previous ones that used more reductive reagents: in the former case, C–C coupling (functionalization) after C–H activation could proceed stoichiometrically without dichloroalkane oxidant,[24] while in the latter case with more reductive reagents (see above), although C–H activation occurred, C–C coupling did not take place without dichloroalkane oxidant.[16] These experimental results strongly imply that different iron active species are responsible for C–H activations when reductively different reagents are employed, and it is very likely that the iron oxidation state in the case with more reductive reagents is lower than that with less reductive reagents, which hence naturally necessitates the dichloroalkane oxidant in the former case to promote the iron oxidation state for the subsequent C–C coupling process. To address this possibility, Fe(III) was also considered in our theoretical study of C–H activation and subsequent C–C coupling.

Concerning low-valent Fe(0), assuming its direct involvement in the C–H activation process through the experimentally known oxidative addition mechanism[9,10] (a formal Fe(0) to Fe(II) process) contrasts sharply with the experimental fact that 1 equiv of organozinc reagent (providing 1 equiv of phenyl anion) is consumed to act as a quantitative H-atom acceptor for C–H activation, as revealed in deuterium-labeling experiments.[47] In the present theoretical modeling of low-valent Fe(II), Fe(III), Fe(I), and Fe(0), we discovered that both Fe(II) and Fe(III) are able to effectively promote the C–H


DOI: 10.1021/jacs.5b12150
J. Am. Chem. Soc. 2016, 138, 3715−3730

**Scheme 2. Four Proposed Catalytic Cycles Studied in This Work for the Low-Valent Iron-Catalyzed Arylation Reaction, with the C−H Activation and C−C Coupling Steps Mediated by (a) Fe(II) and Fe(II), (b) Fe(II) and Fe(III), (c) Fe(I) and Fe(III), and (d) Fe(III) and Fe(III), Respectively**

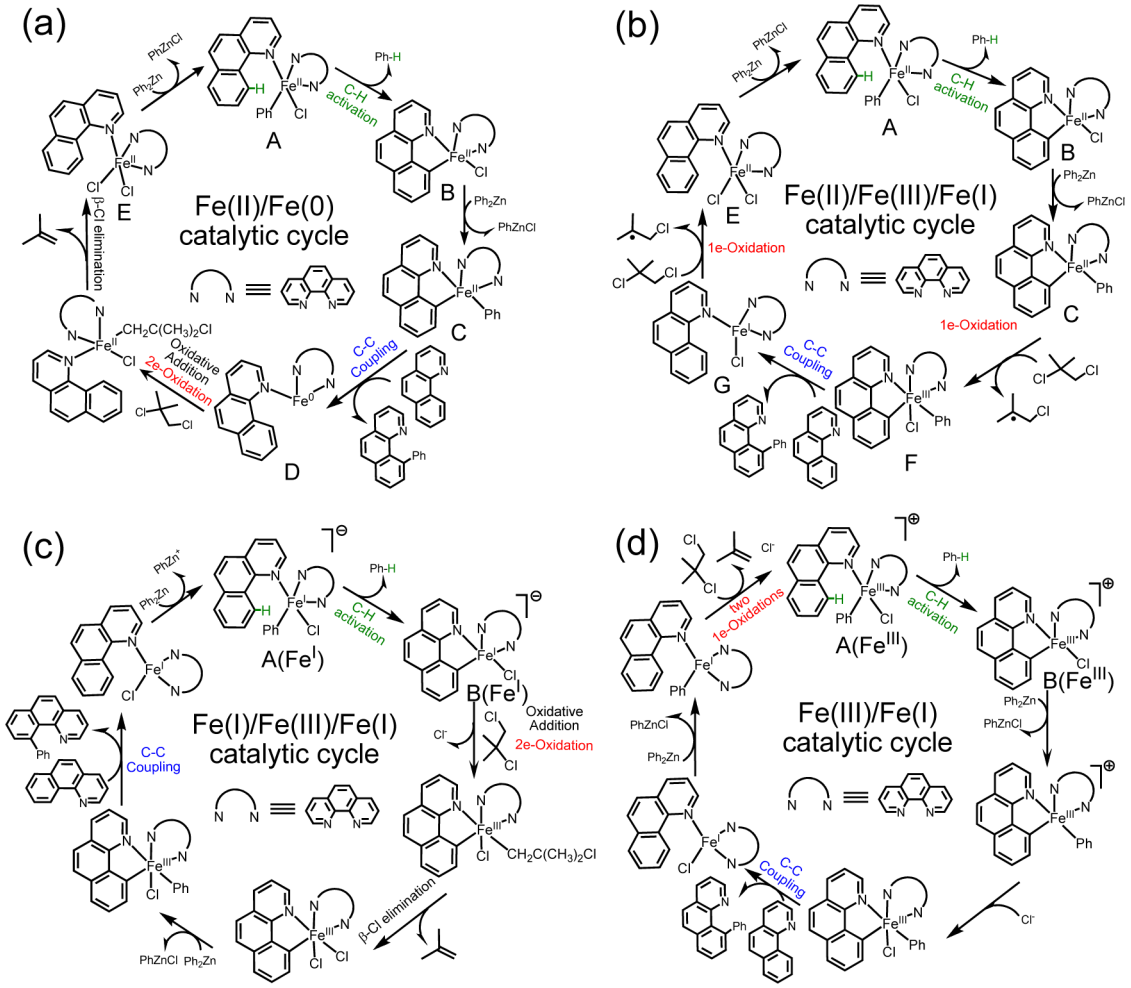


activation process through TSR scenarios. In addition, for initiation of the subsequent C−C coupling process in the C−H functionalization, our calculations suggest the involvement of Fe(III) species generated through one-electron oxidation of the Fe(II) complex by an oxidant like 1,2-dichloroisobutane (DCIB). In comparison, the direct C−C coupling from Fe(II) species is energetically much unfavorable.

Scheme 2 depicts several possible catalytic cycles for the low-valent iron-catalyzed arylation reaction that were studied here. Since the evolution of the iron oxidation state in the catalytic cycle from C−H activation to C−C coupling is still very unclear, our modeling considered a variety of possible oxidation states for C−H activation: Fe(II) (Scheme 2a,b), Fe(I) (Scheme 2c), Fe(III) (Scheme 2d), and Fe(0). We also explored Fe(II) (Scheme 2a) and Fe(III) (Scheme 2b−d) for C−C coupling.

Thus, for example, the mechanism shown in Scheme 2a is initiated from the substrate-bound complex $Fe^{II}$(substrate)(phen)(Ph)Cl (**A**) that contains a phenyl-bound $Fe^{II}$, a phen ligand, and the substrate to be activated ($\alpha$-benzoquinoline), as used by Nakamura and co-workers.[13] This complex **A** undergoes C−H activation via a $\sigma$-bond metathesis mode, liberating Ph−H and forming cyclometalated Fe(II) intermediate **B**. Subsequently, **B** undergoes transmetalation with an organozinc reagent that transfers another phenyl group to the Fe(II) center, forming intermediate **C**. Finally, the reductive elimination of cyclometalated phenyliron(II) intermediate **C** leads to C−C coupling and produces the arylated product. The product is then is replaced by another $\alpha$-benzoquinoline substrate, generating the Fe(0) complex **D**, which undergoes oxidation by DCIB to regenerate the Fe(II) dichloride species **E** with the corresponding alkene. The resting state **A** is then regenerated by phenyl transfer to **E** from the organozinc reagent. In general, this proposed catalytic cycle is a Fe(II)/Fe(0) cycle.

In all of the catalytic cycles in Scheme 2, at most one iron-bound phenyl group is present in the intermediates. Our calculations indicate that transmetalation of a second Ph to **A** to generate $Fe^{II}$(substrate)(phen)$Ph_2$ would lead to dissociation of the substrate from the iron center, probably due to large the steric repulsion between the ligands of iron in $Fe^{II}$(substrate)(phen)$Ph_2$. This result implies that a diphenyliron intermediate like $Fe^{II}$(substrate)(phen)$Ph_2$, which potentially can generate the biphenyl byproduct and disrupt the catalytic cycle, is less likely to be involved during C−H activation of the substrate. Experimentally, Nakamura and co-workers recently discovered that slow addition of the Grignard reagent, which avoids its high concentration in the reaction solution, is a key experimental procedure to successfully make use of the more reactive Grignard reagent in low-valent iron-catalyzed C−H


DOI: 10.1021/jacs.5b12150
J. Am. Chem. Soc. 2016, 138, 3715−3730

activation/functionalization,[16,20,22] which was also used by Cook and co-workers in their experiments.[17,18] In line with our above calculations, this experimental procedure for the Grignard reagent, which is a more efficient Ph-group transfer reagent, also suggests that the second transmetalation of a Ph group is not beneficial to the reaction. On the basis of all the foregoing evidence, our reaction model contains only a single phenyl group coordinated to iron.

*3.1.1. C−H Activation. 3.1.1.1. C($sp^2$)−H Activation by Fe(II).* To explore the mechanism of iron-mediated C−H activation, we first studied the $sp^2$ C−H bond activation in the arylation reaction discovered by Nakamura and co-workers.[13] The DFT-calculated reaction profiles for the Fe(II)-promoted C−H activation step are depicted in Figure 1. All three possible

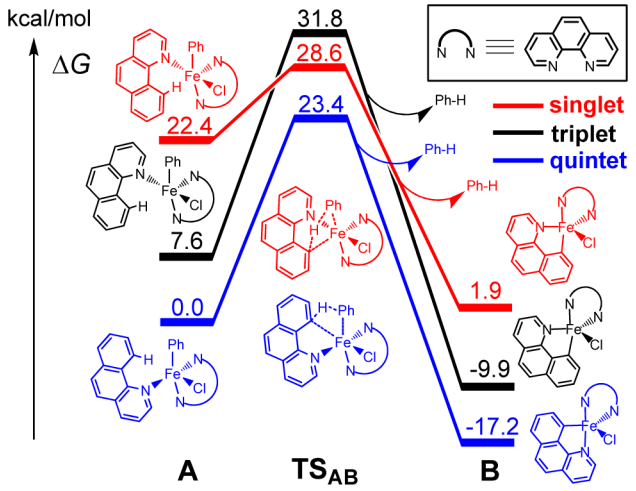


**Figure 1.** DFT-calculated reaction profiles of initial directed $sp^2$ C−H bond activation on all three spin states of Fe(II) in the phenylation reaction. The coordination conformation that has the lowest-energy TS is shown for each spin state.

spin states of Fe(II) were investigated, i.e., the singlet ($S$ = 0), triplet ($S$ = 1), and quintet ($S$ = 2) states. Hereafter we use superscripts 1/3/5 and 2/4/6 on the left-hand side of a given species (e.g., $^{1/3/5}$**A**) to denote the singlet/triplet/quintet and doublet/quartet/sextet spin states, respectively. The substrate-bound phenyliron(II) reactant complex **A** has a high-spin ($S$ = 2) quintet ground state, $^5$**A**, that lies below the triplet and singlet states by 7.6 and 22.4 kcal/mol in Gibbs free energy, respectively. Thus, the three spin states of reactant **A** maintain the following energy order, $^5$**A** < $^3$**A** < $^1$**A**. The three C−H activation transition states $\mathbf{TS_{AB}}$ linking **A** and **B** on the potential energy surfaces (PESs), however, exhibit a different energy ordering, $^5\mathbf{TS_{AB}} < {}^1\mathbf{TS_{AB}} < {}^3\mathbf{TS_{AB}}$, which indicates that along the reaction coordinate $^1\mathbf{TS_{AB}}$ enjoys much more stabilization relative to the corresponding triplet and quintet species. The relative energy data in Figure 1 indicate that this stabilization is as large as about 17−18 kcal/mol compared with both the quintet and triplet states, which leads to an intrinsic C−H activation barrier $\Delta G_S^{\ddagger}$ of only 6.2 kcal/mol on the singlet-state PES from $^1$**A** via $^1\mathbf{TS_{AB}}$. This barrier $\Delta G_S^{\ddagger}$ is very small compared with the corresponding much larger 23.4 and 24.2 kcal/mol barriers on the quintet ground state ($\Delta G_Q^{\ddagger}$) and triplet excited state ($\Delta G_T^{\ddagger}$) PESs, respectively. This TS stabilization of the low-spin singlet state is the most notable feature of this Fe(II)-mediated C−H activation. At our DFT calculation level, because of the large quintet−singlet spin-state gap in the reactant **A**, this stabilization still cannot make $^1\mathbf{TS_{AB}}$ the lowest TS among the three C−H activation TSs.

Approximate density functionals are known to poorly account for the relative spin-state energetics of Fe(II) complexes.[48] To improve the accuracy of our adopted DFT protocol, we carried out expensive open-shell CCSD(T) calculations to obtain the corresponding spin-state energetics and C−H activation barriers at the CCSD(T)/CBS level including the iron 3s3p core−valence correlation effect. The comparative CCSD(T) and DFT results for the C−H activation step based on the same simplified model shown in Figure 2a are depicted in Figure 3a. Compared with the

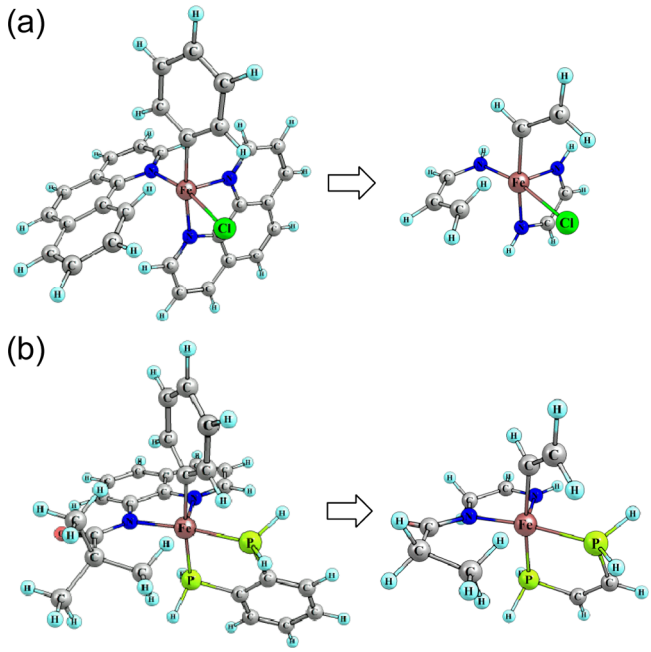


**Figure 2.** Truncated models for high-level coupled cluster calculations obtained from the corresponding ones used in DFT calculations for (a) $sp^2$ C−H activation in Figure 1 and (b) $sp^3$ C−H activation in Figure 5.

CCSD(T) reference data, we note the following features of the DFT results: (a) B3LYP significantly overestimates the singlet−quintet gap $\Delta G_{gap}^{S-Q}$ for the C−H activation reactant complex (**A**) by 14.0 kcal/mol while underestimating the triplet−quintet gap $\Delta G_{gap}^{T-Q}$ by 7.7 kcal/mol. (b) The C−H activation barriers on the singlet- and quintet-state profiles ($\Delta G_S^{\ddagger}$ and $\Delta G_Q^{\ddagger}$) are reasonably calculated by B3LYP, such that DFT overestimates these barriers by only 2.3 and 4.2 kcal/mol, respectively, whereas the barrier on the triplet state PES ($\Delta G_T^{\ddagger}$) is overestimated by 12.0 kcal/mol. With these corrections from the CCSD(T) calculations, the refined reaction energy profiles of the C−H activation step for the actual system used in the experiments of Nakamura and co-workers,[13] which represent our most reliable final picture of the corresponding $sp^2$ C−H activation by Fe(II), are shown in Figure 3b. It can be seen that as a result of the CCSD(T) corrections, $^1\mathbf{TS_{AB}}$ becomes the lowest-lying TS for C−H activation among all three spin states. Thus, starting from the quintet ground state RC $^5$**A**, a spin-state transition to the singlet surface has to occur during this energetically most favorable C−H activation pathway. In this manner, the effective activation barrier $\Delta G_{eff}^{\ddagger}$ for going from $^5$**A** to $^1\mathbf{TS_{AB}}$ is only 12.3 kcal/mol. This is catalysis by spin


DOI: 10.1021/jacs.5b12150
J. Am. Chem. Soc. 2016, 138, 3715−3730

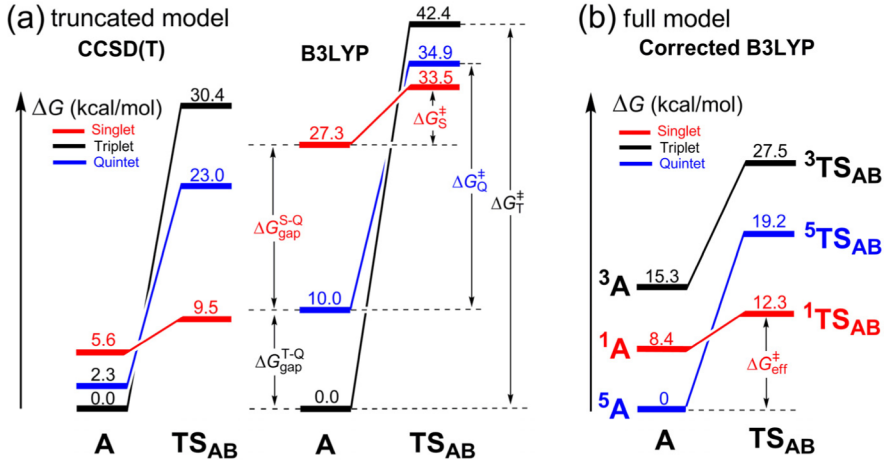


**Figure 3.** (a) Comparative results for the $sp^2$ C−H activation step from CCSD(T) and B3LYP calculations, both based on the truncated model in Figure 2a. (b) B3LYP results for the $sp^2$ C−H activation step in Figure 1 after addition of the CCSD(T) corrections from the truncated model.

crossover as envisioned originally by one of us and his co-workers.[30,31a] On the contrary, the triplet state is not likely to be involved during the C−H activation since it remains above the singlet and quintet PESs.

*This reaction picture is a typical TSR scenario.* Interestingly, in biological or bioinorganic high-valent iron(IV)−oxo systems, where C−H activation reactivity is also controlled by a TSR scenario, it is the high-spin state ($S$ = 2) rather than the low-spin state ($S$ = 0) that internally catalyzes the reaction. Since different ligation environments with different ligand field strengths can selectively stabilize either high-spin or low-spin states of iron, this difference between high-valent and low-valent iron in C−H activation reactivity may necessitate a different ligation strategy to improve the C−H activation reactivity, which then has significant diverse influences on the future development in these two areas in bioinorganic and organometallic iron chemistry.

**What are the origins of internal catalysis in the singlet state?** Inspection of the TS structures in Figure 1 shows that the low-valent iron species adopts a $\sigma$-bond-metathesis-type reaction mode[49] for C−H activation. This is in sharp contrast to the H-abstraction mechanism whereby high-valent iron−oxo species perform C−H bond activation.[31] This difference most likely originates from the fact that Fe(IV)═O has oxyl (Fe−O$^{\bullet}$) character and thus can easily abstract a hydrogen atom to form a strong O−H bond. In contrast, a potential H abstraction by low-valent iron complexes would generate a weak Fe−H bond, which cannot compensate for the energy consumption required for the C−H bond breakage in the H-atom transfer (HAT) process. Therefore, the low-valent Fe(II) complex assumes an alternative structure in which the $\sigma$-bond metathesis C−H activation pathway creates an Fe−C bond, which is stronger than an Fe−H bond and bears a known strength correlation with the broken C−H bond,[50,51] along with a strong C−H bond in the liberated Ph−H during the original C−H activation. Therefore, the $\sigma$-bond metathesis in the low-valent iron systems is thermodynamically more favored over H abstraction during C−H activation.

In addition, there is a kinetic TS effect that prefers the low-spin state of Fe(II) over the higher-spin congeners for the C−H activation. Thus, as shown in the orbital cartoons in Scheme 3a, this reactivity advantage of low-spin iron over high-spin iron can be understood in terms of favorable donation/back-donation orbital interactions between the metal, the C−H bond, and the H-atom acceptor (phenyl ligand). Thus, the Fe−CH agostic interaction is favorable for the low-spin singlet state of Fe(II) because it involves two orbital interactions between a filled orbital and a vacant orbital. One of these is the $\sigma_{CH}$−$d_{z^2}$ interaction, and the other is the $\sigma_{hyb(Ph)}$−$\sigma_{CH}$* interaction between the doubly occupied $\sigma$ hybrid of the phenyl ligand and the vacant antibonding orbital of the C−H bond undergoing activation. Since the $d_{z^2}$ orbital is singly occupied in the triplet and quintet states (see Scheme 3b), the $\sigma_{CH}$−$d_{z^2}$ interaction involves three electrons and can even be destabilizing. Therefore, the higher-spin transition states are much less stabilized by orbital interactions compared with the singlet state. The structures of $^{1/3/5}$**TS$_{AB}$** on three spin states are depicted in Figure 4, from which we can observe the stronger Fe−CH interaction in $^{1}$**TS$_{AB}$**, leading to shorter Fe−C and Fe−H distances that stabilize the singlet state $^{1}$**TS$_{AB}$** compared with the other two spin cases. Interestingly, it has long been known

**Scheme 3. (a) Donation/Back-Donation Orbital Interactions between Fe(II), the C−H $\sigma$ Bond, and the Carbon of the Phenyl Group (the H Acceptor in C−H Activation); (b) Fe(II) 3d Shell Occupancies in an Octahedral Coordination Environment for Low-, Medium-, and High-Spin States**

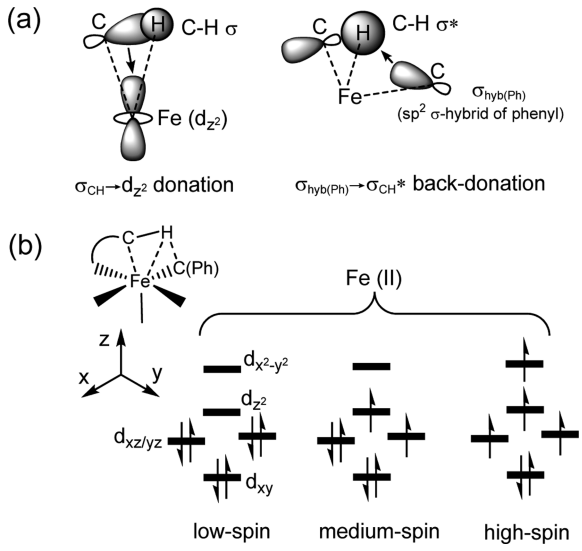




DOI: 10.1021/jacs.5b12150
J. Am. Chem. Soc. 2016, 138, 3715−3730

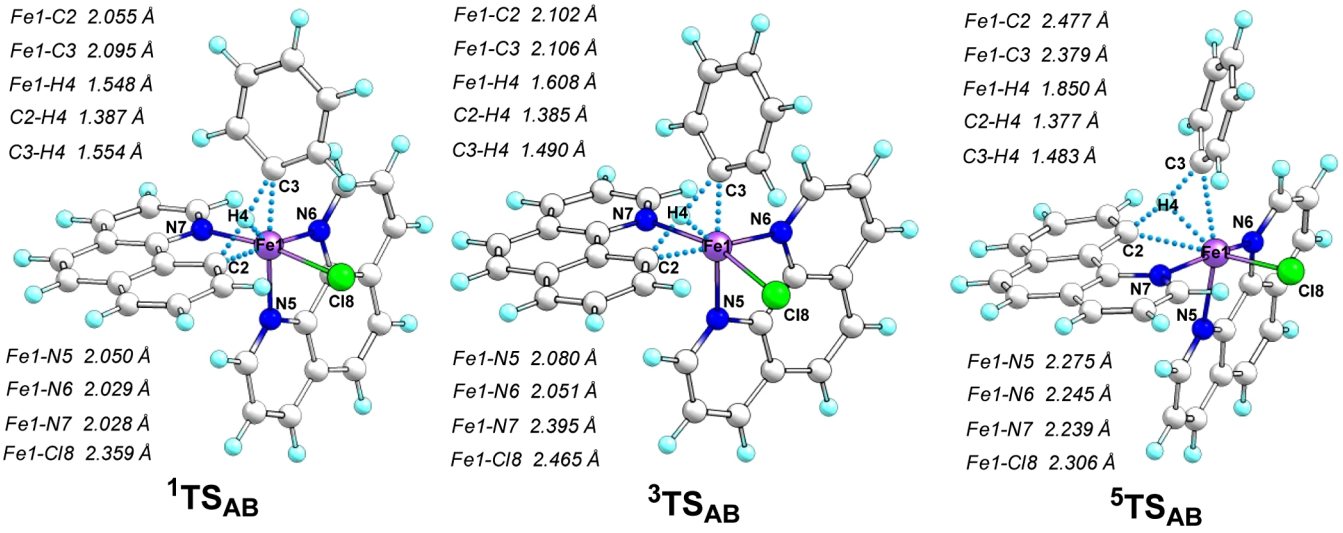


**Figure 4.** Structures of the low-, medium-, and high-spin C($sp^2$)–H activation TSs mediated by Fe(II) with key bond distances labeled.

that the low-spin state of a metal center can beneficially promote C–H activation via the oxidative addition mechanism.[52] However, for C–H activation in the $\sigma$-bond metathesis mode, to the best of our knowledge this is the first time that the low-spin state has been found to have an apparent advantage over high-spin states.

*3.1.1.2. C($sp^3$)–H Activation by Fe(II).* As reported by Nakamura and Ackermann,[25,26] aliphatic $sp^3$ C–H bonds are also amenable to activation by low-valent iron complexes. We studied the corresponding C–H activation step for all three spin states employing a catalytic system based on the experimental work of Nakamura and co-workers.[26] As shown in Figure 5, singlet-state TS stabilization is also apparent for $sp^3$ C–H activation. The DFT-calculated barrier ($\Delta G_S^{\ddagger}$) to go from $^1\mathbf{A}(\mathbf{sp^3})$ to $^1\mathbf{TS_{AB}}(\mathbf{sp^3})$ on the singlet-state PES is 14.6 kcal/mol, which can be compared with $\Delta G_Q^{\ddagger}$ = 37.6 kcal/mol to go from $^5\mathbf{A}(\mathbf{sp^3})$ to $^5\mathbf{TS_{AB}}(\mathbf{sp^3})$ on the quintet-state PES. This TS stabilization of about 23 kcal/mol makes $^1\mathbf{TS_{AB}}(\mathbf{sp^3})$ the energetically lowest TS among the three C–H activation TSs.

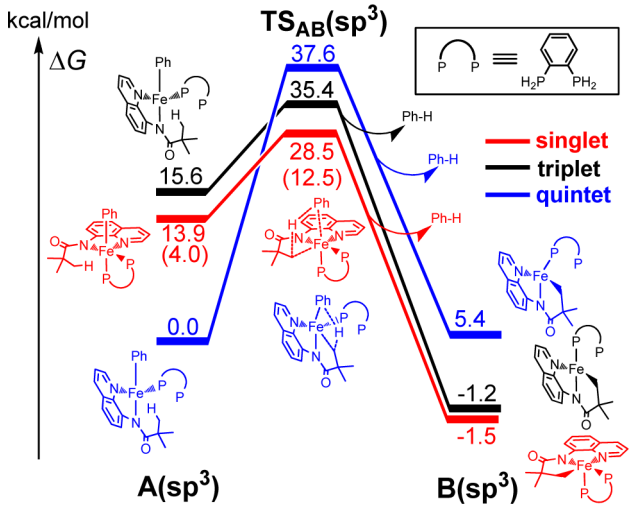


**Figure 5.** B3LYP calculated reaction profiles for $sp^3$ C–H activation step on all three spin states. The relative energetics after adding CCSD(T) correction based on simplified model shown in Figure 2b are labeled in parentheses.

Thus, for C–H activation with a different ligand environment from the $sp^2$ one, *a TSR scenario similar to that for $sp^2$ C–H activation transpires also for an $sp^3$ C–H bond. This demonstrates that TSR is not dependent on a specific ligand environment but should be a common feature to all Fe(II)-mediated C–H activations.* It is notable that for more inert $sp^3$ C–H activation, the intrinsic barrier on the singlet-state PES ($\Delta G_S^{\ddagger}$ = 14.6 kcal/mol) is larger than the corresponding one for $sp^2$ C–H activation shown in Figure 1 (6.2 kcal/mol). We also calculated the kinetic isotope effect (KIE) for $sp^3$ C–H activation, in which the $CH_3$ group to be activated in C–H activation was replaced by $CD_3$. The computed KIE of 3.7 via $^1\mathbf{TS_{AB}}(\mathbf{sp^3})$ further matches the experimental datum, KIE = 4.0,[26] whereas the one via the quintet TS produces a KIE of 4.9, which provides additional support for the TSR scenario here.

The DFT energetics of the $sp^3$ C–H activation process was also improved by adding corrections from the open-shell CCSD(T) calculations on a simplified model (see Figure 2b). The corrected values are shown in Figure 5 in parentheses. Thus, the key singlet–quintet gap $\Delta G_{gap}^{S-Q}$ changed from 13.9 to 4.0 kcal/mol, and the effective activation barrier $\Delta G_{eff}^{\ddagger}$ from the quintet ground state RC $^5\mathbf{A}(\mathbf{sp^3})$ through TS $^1\mathbf{TS_{AB}}(\mathbf{sp^3})$ dropped from 28.5 to 12.5 kcal/mol, which can be compared with the corresponding $\Delta G_{gap}^{S-Q}$ of 8.4 kcal/mol and $\Delta G_{eff}^{\ddagger}$ of 12.3 kcal/mol for the $sp^2$ C–H activation process. In summary, we found that *both $sp^3$ and $sp^2$ C–H activations promoted by Fe(II) proceed via the same TSR scenario.*

*3.1.1.3. C–H Activation by Fe(I) and Fe(0).* Since Fe(I) is also possibly present in the reductive reaction environment as proposed by Bedford for Fe-catalyzed cross-coupling reactions,[46] we further explored the C–H activation by an Fe(I) complex. The calculated reaction profiles are shown in Figure 6. First, one can see from Figure 6 that the relative free energies of all three C–H activation TSs ($\mathbf{TS_{AB}}(\mathbf{Fe^I})$) for the doublet/quartet/sextet spin states in the Fe(I) case (i.e., 37.7/38.0/30.0 kcal/mol) are higher than the relative free energies of the corresponding TSs ($\mathbf{TS_{AB}}$) for the singlet/triplet/quintet spin states in the Fe(II) case (28.6/31.8/23.4 kcal/mol; Figure 1). This result demonstrates that Fe(II) is more reactive in C–H activation than the further-reduced Fe(I) active center.

Curiously, genuine Fe(I) possesses a $d^7$ configuration and in principle should not have a sextet spin state since the $d^7$


DOI: 10.1021/jacs.5b12150
J. Am. Chem. Soc. 2016, 138, 3715–3730

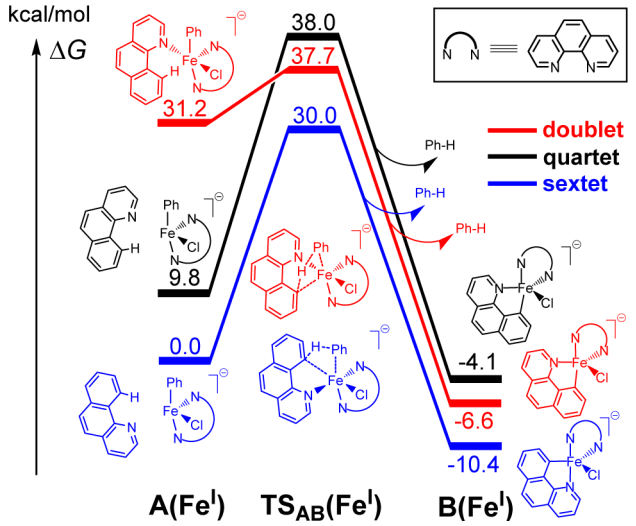


**Figure 6.** DFT-calculated reaction profiles of initial directed sp$^2$ C−H bond activation on all three spin states of Fe(I) in the phenylation reaction. Energies were not corrected with CCSD(T).

configuration can have at most three unpaired electrons in the 3d subshell, corresponding to a quartet state. Importantly, the reason for the presence of a sextet state was found to be that all three Fe(I) species in our DFT calculations are not genuine Fe(I) species but are actually Fe(II) states plus a $\pi$ radical anion on the phen ligand. Previous theoretical calculations based on the same B3LYP functional had generated the genuine Fe(I) electronic structure with a very different phosphine-rich ligating environment in the iron-catalyzed cross-coupling reaction,[53] and hence, the presently found Fe(II)−[phen]$^{\bullet-}$ electronic structure should not be attributed necessarily to DFT errors. Moreover, this electronic structure of Fe(II) plus phen $\pi$ radical anion was conserved even after we removed the chloride anion ligand from the system to make it neutral, like the neutral genuine Fe(I) complex characterized before;[53] this demonstrated that it is not the negative charge of the system that causes the appearance of a ligand-based radical. This result further implies that in our system under study, genuine Fe(I) is not likely to be relevant in catalysis. Finally, it is notable that after Fe(II) is reduced to nongenuine Fe(I), the interactions between the substrate and iron become weaker, causing the substrate to dissociate from iron in the quartet and sextet states, which should be detrimental to the C−H activation. In total, our above results do not support the Fe(I)-mediated C−H activation mechanism. Nevertheless, it is interesting to note that radical anion/cation ligands, which are also called "redox-active" or "non-innocent" ligands, are considered in many other examples to play important roles in TM catalysis, e.g., conferring nobility on base-metal (Fe, Co, Ni) catalysts.[54]

Since many recent experimental and theoretical studies on low-valent cobalt-catalyzed C−H activation have suggested that Co(0) is likely to be the active species for C−H activation,[55,56] sometimes via a mechanism other than oxidative addition,[57] it was intriguing to explore whether Fe(0) is also a competent active species in the current case of C−H activation. To test this possibility, we calculated the two-electron-reduced **A**. Interestingly, after extensive calculations for various possible electronic configurations, we found that in our studied system Fe invariably ends up adopting the Fe(II) state. At the same time, the phen ligand and substrate ($\alpha$-benzoquinoline), both of which possess large $\pi$-conjugated aromatic rings, assume $\pi$ radical anion states. Thus, the formal Fe(0) system is in fact Fe(II) plus two $\pi$ radical anions and hence should exhibit the Fe(II) reactivity, as in the formal Fe(I) system demonstrated above. Indeed, as shown in Figure S1 in the Supporting Information, the calculated C−H activations by this formal Fe(0) system are less favorable than those by the Fe(II) system shown in Figure 1. On the basis of these results, in the catalytic system under study we do not support the participation of a formal Fe(0) as an active species in C−H activations promoted by low-valent iron.

*3.1.1.4. C−H Activation by Fe(III).* As suggested by Nakamura and co-workers, with less reductive organoboron or organoaluminum reagents, Fe(III) may mediate the C−H activation.[24,27] To test this proposal, we computed C−H bond activation mediated by Fe(III) species. The results are displayed in Figure 7. It was intriguing to find that similar to

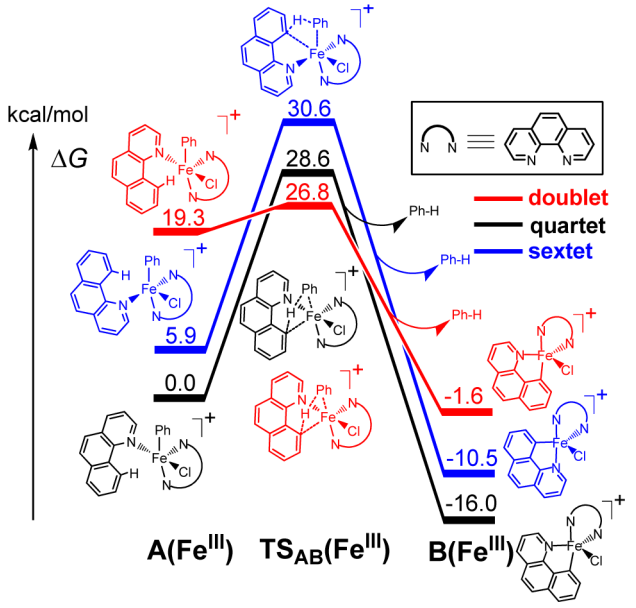


**Figure 7.** DFT-calculated reaction profiles of initial directed sp$^2$ C−H bond activation on all three spin states of Fe(III) in the phenylation reaction. Energies were not corrected with CCSD(T).

the Fe(II) case, the low-spin doublet ($S = {}^1/_2$) Fe(III) also can mediate the sp$^2$ C−H activation with significant TS stabilization, as shown by the intrinsic barrier $\Delta G_D^{\ddagger}$ of 7.5 kcal/mol on the doublet-state surface. This is comparable to the calculated $\Delta G_S^{\ddagger}$ of 6.2 kcal/mol for Fe(II) at the same DFT computational level. Thus, although the low-spin state $^2$**A**(**Fe$^{III}$**) is not the lowest-energy reactant state, the corresponding TS $^2$**TS$_{AB}$**(**Fe$^{III}$**) becomes the lowest-energy TS, which has an effective activation barrier $\Delta G_{eff}^{\ddagger}$ of 26.8 kcal/mol measured from the ground-state sextet reactant $^6$**A**(**Fe$^{III}$**). This $\Delta G_{eff}^{\ddagger}$ value is slightly smaller than the corresponding $\Delta G_{eff}^{\ddagger}$ of 28.6 kcal/mol at the same DFT level for the Fe(II) system shown in Figure 1. Thus, Fe(III) complexes can promote C−H activation even more efficiently than the Fe(II) congeners. *Most importantly, our results indicate that both Fe(II)- and Fe(III)-promoted C−H bond activations transpire via TSR scenarios.* Thus, we conclude that in the presence of Fe(III) in the reaction system, the ferric species possesses sufficient reactivity to promote the C−H activation.

*3.1.2. C−C Coupling.* Following C−H activation by Fe(II) complexes, which according to our calculations is most likely to


DOI: 10.1021/jacs.5b12150
J. Am. Chem. Soc. 2016, 138, 3715−3730

be promoted through a TSR scenario, the next important step in the C−H phenylation reaction is C−C coupling. To explore the mechanism of C−C coupling, we considered pathways mediated by both Fe(II) and Fe(III) intermediates, the results of which are presented below separately.

*3.1.2.1. C−C Coupling via the Fe(II) Complex.* As shown in Scheme 2a,b, the low-valent Fe(II)-mediated C−H bond cleavage generates cyclometalated Fe(II) intermediate **B**, which has a quintet ground state ($^5$**B**). To proceed with the C−C coupling to afford the final C−H arylated product, transmetalation of a phenyl group from the organozinc reagent to iron(II) is required, as shown in Figure 8. After this

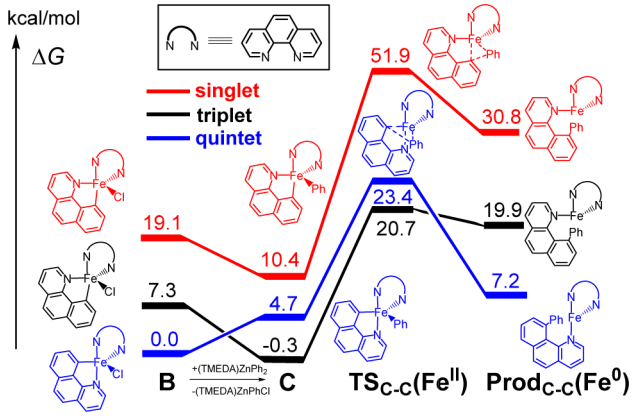


**Figure 8.** DFT-calculated reaction profiles of phenyl transmetalation from **B** and subsequent C−C coupling (reductive elimination) from the Fe(II) intermediate on all three spin states in the phenylation reaction. Energies were not corrected with CCSD(T).

transmetalation, which is thermodynamically exothermic on the singlet- and triplet-state PESs but endothermic on the quintet-state PES, diaryliron(II) intermediate **C** is formed, with the triplet state ($^3$**C**) as the ground state. From $^3$**C** through $^3$**TS**$_{C-C}$(**Fe**$^{II}$), a diaryl C−C coupling via reductive elimination produces the Fe(0) product, **Prod**$_{C-C}$(**Fe**$^0$), with a substantial barrier of 21.0 kcal/mol. Alternatively, the C−C coupling on the quintet-state surface through $^5$**TS**$_{C-C}$(**Fe**$^{II}$), which lies 2.7 kcal/mol above $^3$**TS**$_{C-C}$(**Fe**$^{II}$), also needs to overcome a substantial barrier of 18.7 kcal/mol. On the singlet-state surface, the C−C coupling turns out to be even more difficult since the reductive elimination barrier is more than 40 kcal/mol. Besides the high barriers for C−C coupling mediated by Fe(II), its reaction energies also fail to provide enough driving force for this C−C coupling step. All three reaction energies from **C** to **Prod**$_{C-C}$(**Fe**$^0$) on the three spin-state surfaces are positive, with those for the triplet and singlet state being endothermic by more than 20 kcal/mol. All of these data demonstrate that C−C coupling from Fe(II) can be neither kinetically nor thermodynamically favorable. This conclusion is generally in line with previous experimental discoveries of sluggish reductive elimination reactivity for C−C coupling from diaryl/dialkyl/dialkenyl/dialkynyl Fe(II) complexes.[58,59]

Concerning the transmetalation of a phenyl group from the organozinc reagent, several interesting phenomena were observed in the experiments.[13] Nakamura and co-workers found that only one of the two phenyl groups of the organozinc reagent ($ZnCl_2$ + 2PhMgBr) was utilized in the reaction and that the diamine ligand *N*,*N*,*N*′,*N*′-tetramethyl-1,2-ethylenediamine (TMEDA) and $Mg^{2+}$ are quite beneficial when used with the organozinc reagent for the C−H arylation reaction. To explore the root causes for these findings, we comparatively calculated the free energy changes, i.e., the driving forces for the transmetalation processes. As shown in Scheme 4, through calculations we found that (a) the use of TMEDA as the ligand of zinc can increase the driving force for the zinc-to-iron transmetalation process from $^5$**B** to $^3$**C** by 5.9 kcal/mol, (b) the first phenyl group of the organozinc reagent has a larger tendency to undergo transmetalation than the second one by bearing a reaction driving force advantage of 6.3 kcal/mol, and (c) $Mg^{2+}$ can slightly further enhance the driving force for the transmetalation process by about 1 kcal/mol. Thus, these three experimentally observed factors all play roles in adjusting the reactivity of the organozinc reagent in the transmetalation, which explains the experimental findings of Nakamura and co-workers.[13]

*3.1.2.2. C−C Coupling via the Fe(III) Complex.* Generally, the above results demonstrate that direct C−C coupling from diaryliron(II) intermediates is neither thermodynamically nor

**Scheme 4. Calculated Reaction Thermodynamics of the Zinc-to-Iron Transmetalation Process from $^5$B to $^3$C Affected by the Factors of (a) TMEDA, (b) the First and Second Phenyl Groups, and (c) $Mg^{2+}$** [a]

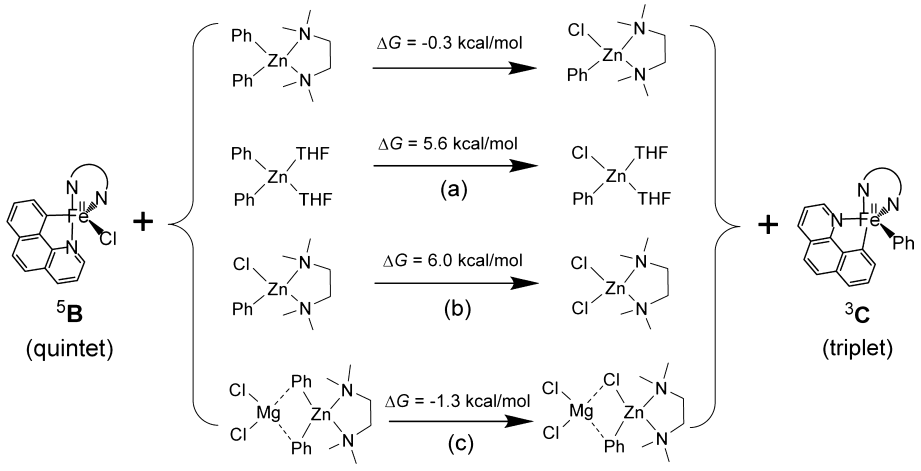


[a]For open-shell species with multiple spin states, the lowest-energy one was selected.



DOI: 10.1021/jacs.5b12150
J. Am. Chem. Soc. 2016, 138, 3715−3730

**Scheme 5. (a) Calculated Free Energy Driving Force ($\Delta G$) for SET Oxidation of $^3$C by DCIB and (b) Calculated $\Delta G$ and Barrier ($\Delta G^{\ddagger}$) for C−C Coupling by Reductive Elimination from $^3$C[a]**

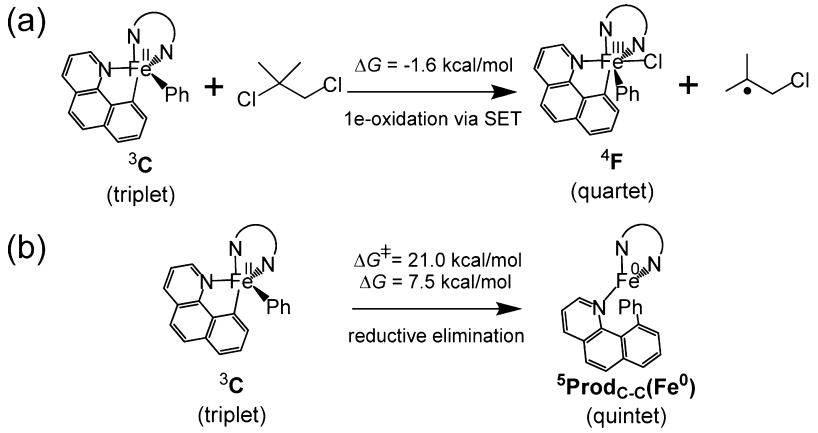


[a]For open-shell species with multiple spin states, the lowest-energy one was selected.

kinetically favorable. This raises an intriguing question: what could be a reasonable mechanism for this C−C coupling step? For the C−C coupling reaction from diaryliron(II) complexes such as **C** in the presence of halogenated alkane oxidant, there could be an alternative mechanism via one-electron oxidation of Fe(II) to Fe(III) in which single-electron transfer (SET) from the iron(II) intermediate **C** to the alkyl halide would cause C−halogen bond cleavage and generate the corresponding alkyl radical, as proposed previously for many four-coordinate Fe(II) centers.[59,60] We carried out calculations to test the possibility of a SET reaction in the five-coordinate species **C**. We computed the free energy driving force for SET from the lowest-energy species $^3$**C** to the oxidant DCIB. This SET affords the ferric chloride complex $^4$**F** and the monochloroalkyl radical species, as shown in Scheme 5a. This process was compared with reductive elimination from $^3$**C**, which is shown in Scheme 5b. We found that this one-electron oxidation process is thermodynamically more favorable than the reductive elimination process for Fe(II) complex **C**. After this one-electron oxidation, the subsequent reductive elimination from **F** to afford the final phenylated product, as shown in Figure 9, is much more favorable both thermodynamically and kinetically than the reductive elimination directly from Fe(II) intermediate **C**. The lowest barrier and reaction energy for reductive elimination from Fe(III) are 11.3 and −22.6 kcal/mol, respectively, which are much lower than the corresponding values of 21.0 and 7.5 kcal/mol for reductive elimination from Fe(II) shown in Scheme 5b. Thus, our calculations suggest that one-electron oxidation by DCIB followed by reductive elimination from Fe(III) is possibly the C−C coupling mechanism for the phenylation reaction. This result of different oxidation states of iron for C−H activation via Fe(II) and C−C coupling via oxidatively generated Fe(III) is in agreement with the experimental finding by Nakamura and co-workers that without DCIB, although C−H activation occurs, the C−C coupling cannot take place.[16] Notably, our finding of the necessity to involve Fe(III) species in the C−C coupling is also consistent with the current mechanistic understanding of reductive elimination for C−C coupling in iron-catalyzed [2 + 2] cycloadditions of alkenes by Chirik and co-workers.[61]

*3.1.3. Fe(II) Catalyst Regeneration from Fe(I) after C−C Coupling.* The reductive elimination from Fe(III) species **F** for the last C−C coupling step in the C−H functionalization

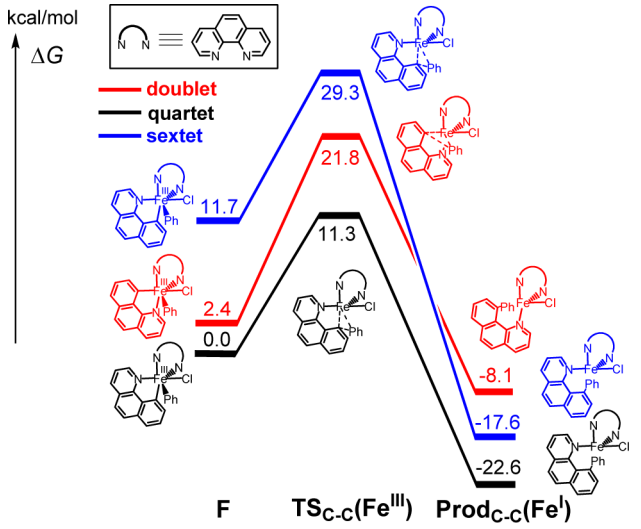


**Figure 9.** DFT-calculated reaction profiles for C−C coupling through reductive elimination from Fe(III) intermediates for all three spin states. Energies were not corrected with CCSD(T).

generates the Fe(I) species **Prod$_{C-C}$(Fe$^{I}$)** containing the phenylated product. Upon substitution of $\alpha$-benzoquinoline into **Prod$_{C-C}$(Fe$^{I}$)**, the product is released and Fe(I) complex **G** containing an updated substrate molecule is formed. Since we have revealed the advantage of Fe(II) over Fe(I) in C−H activation, it is necessary to regenerate the Fe(II) catalyst from **G** for the next round of C−H activation. For this regenerative oxidation step from Fe(I), we explored two pathways. One is a two-electron oxidation process through canonical organometallic oxidative addition of a C−Cl bond of DCIB, which could be followed by the possible $\beta$-Cl elimination to generate an alkene and the Fe(III) dichloride complex. The other is initiated by SET from Fe(I) to DCIB to afford the Fe(II) chloride complex plus the monochloroalkyl radical species. As shown in Scheme 6a,b, we found that the SET pathway is thermodynamically much more favorable than the oxidative addition. Furthermore, compared with DCIB, the monochloroalkyl radical species generated by SET is an even more powerful oxidant (Scheme 6b,c). Via SET, the Fe(I) species **G** [Fe$^{I}$(substrate)(phen)Cl] undergoes oxidation to give Fe(II) intermediate **E** [Fe$^{II}$(substrate)(phen)Cl$_2$], which subsequently


DOI: 10.1021/jacs.5b12150
J. Am. Chem. Soc. 2016, 138, 3715−3730

**Scheme 6. Calculated Free Energy Driving Forces (Reaction Free Energies) of (a) C−Cl Oxidative Addition versus (b, c) SET for Oxidation of Fe(I) Species G to Fe(II) Species E by (b) DCIB and (c) its Monochloroalkyl Radical Generated by SET**[a]

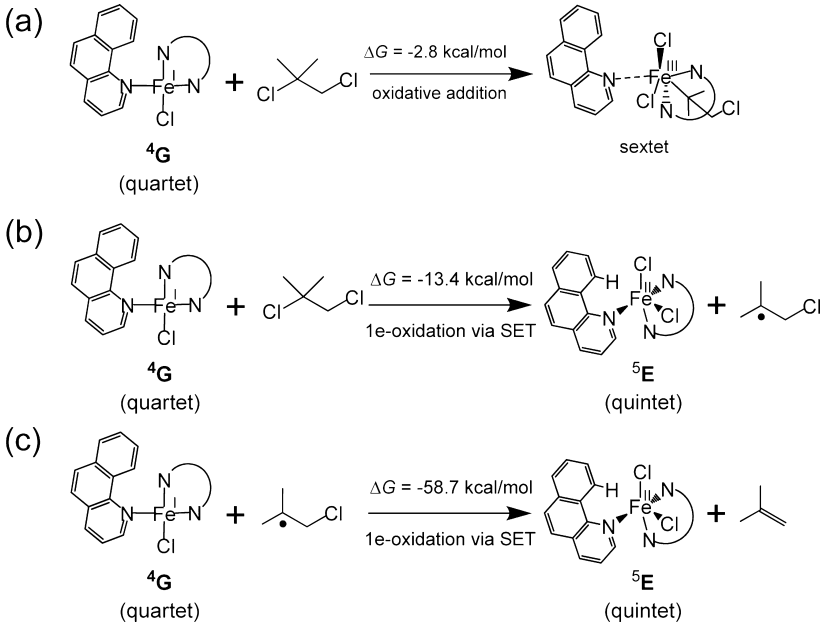


[a]For open-shell species with multiple spin states, the lowest-energy one was selected.

undergoes Ph group transmetalation from the organozinc reagent to regenerate the Fe(II)−phenyl starting intermediate **A** [$Fe^{II}$(substrate)(phen)(Ph)Cl], thus coming full cycle for the phenylation reaction.

*3.1.4. Summary of the Mechanism for the Whole C−H Arylation Reaction.* On the basis of our findings above for the three constituent steps in the low-valent iron-catalyzed C−H functionalization (arylation) reaction, we propose that the mechanism shown in Scheme 2b via an Fe(II)/Fe(III)/Fe(I) catalytic cycle is the most probable catalytic cycle for the low-valent iron-catalyzed C−H arylation reaction with the more reductive reagents, while with the less reductive reagents, the Fe(III)/Fe(I) catalytic cycle shown in Scheme 2d can possibly be a more appropriate alternative.

**3.2. Ligand-Sphere Effects on C−H Bond Activation.** The ligand sphere was found to be a crucial factor in low-valent iron-catalyzed C−H activations. To explore the ligand effect, we considered various ligands (L) shown in Scheme 7,

**Scheme 7. Four Kinds of Ligands Explored in This Study for $sp^2$ C−H Activation**

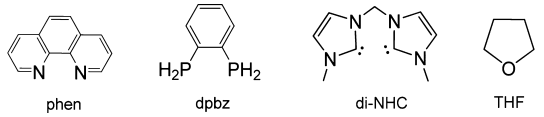


including not only the experimentally employed *N,N*-bidentate dipyridine (phen) and *P,P*-bidentate diphosphine (1,2-bis-(diphenylphosphino)benzene (dppbz), modeled by 1,2-diphosphinobenzene (dpbz)) ligands but also the *C,C*-bidentate dicarbene (di-NHC) ligand, which to the best of our knowledge has not been reported previously. As a reference state, we calculated the complex with two THF solvent molecules as ligands (with O as the coordinating atom). The computed $sp^2$ C−H activation profiles for these four systems with different types of coordinating atoms (N, P, C, or O) to ligate iron are shown in Figure 10.

First of all, comparing Figure 10a−c with Figure 10d, one can see that the most unique effect exerted by the different ligands are the differential stabilization energies of the low-spin singlet-state profiles (red profiles) relative to the high-spin quintet ones (blue profiles). The singlet-quintet gap ($\Delta G_{gap}^{S-Q}$) for C−H activation reactant **A**, which reveals quantitatively this stabilization, decreases from 34.6, to 29.4, 17.7, and 22.4 kcal/mol with THF, di-NHC, dpbz and phen ligands, respectively. Despite the large ligand effect on $\Delta G_{gap}^{S-Q}$, the barrier in the singlet-state profile ($\Delta G_S^{\ddagger}$) is almost unaffected by the various ligands, being 6.3, 7.4, 6.8, and 6.2 kcal/mol for THF, di-NHC, dpbz, and phen, respectively. This result indicates that ligand stabilization for the singlet state is not limited to the C−H activation RC but also extends to the C−H activation TS. In this way, the effective C−H activation barrier ($\Delta G_{eff}^{\ddagger}$) measured from the quintet ground state of the RC is lowered by the ligand effect. It is thus clear that selective stabilization by ligands such as phen and dpbz, which make the singlet state low enough that it cuts through the quintet ground state PES along the C−H activation reaction coordinate, is the crucial factor in promoting C−H activation reactivity. *Hence, it is the suitable ligand that brings about the TSR in Fe(II)-promoted C−H activation.*

Figure 11 reveals the reason why a certain ligand can stabilize the singlet state relative to quintet state. It can be seen that the ligand binds the central Fe(II) much tighter in the singlet state by imposing much shorter metal−ligand bonds than in the quintet state. Thus, the singlet state of Fe(II) favors stronger ligand binding, and consequently, certain ligands with strong ligand fields such as phen and dpbz selectively stabilize the low-spin singlet staten greatly.

From Figure 10a,b, it appears that the diphosphine ligand dpbz could be superior to the dipyridine ligand phen in the Fe(II)-promoted C−H activation because dpbz exerts a larger


DOI: 10.1021/jacs.5b12150
J. Am. Chem. Soc. 2016, 138, 3715−3730

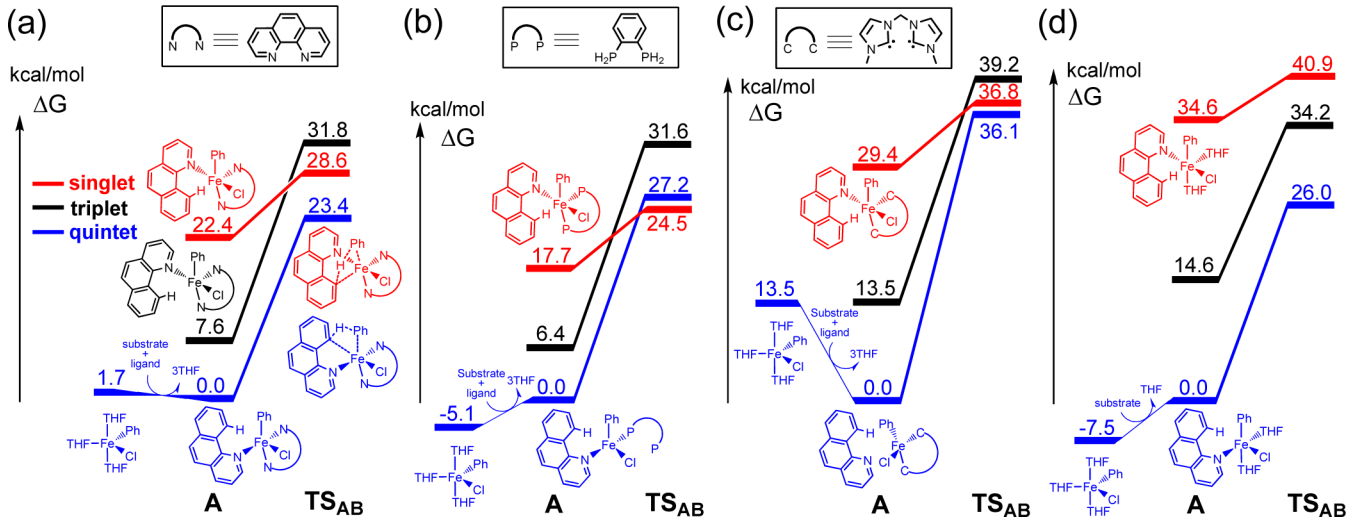


**Figure 10.** Reaction profiles for the Fe(II)-mediated $sp^2$ C−H activation step with different ligands: (a) phen; (b) dpbz; (c) di-NHC; (d) solvent THF (without specially added ligand). Energies were not corrected with CCSD(T).

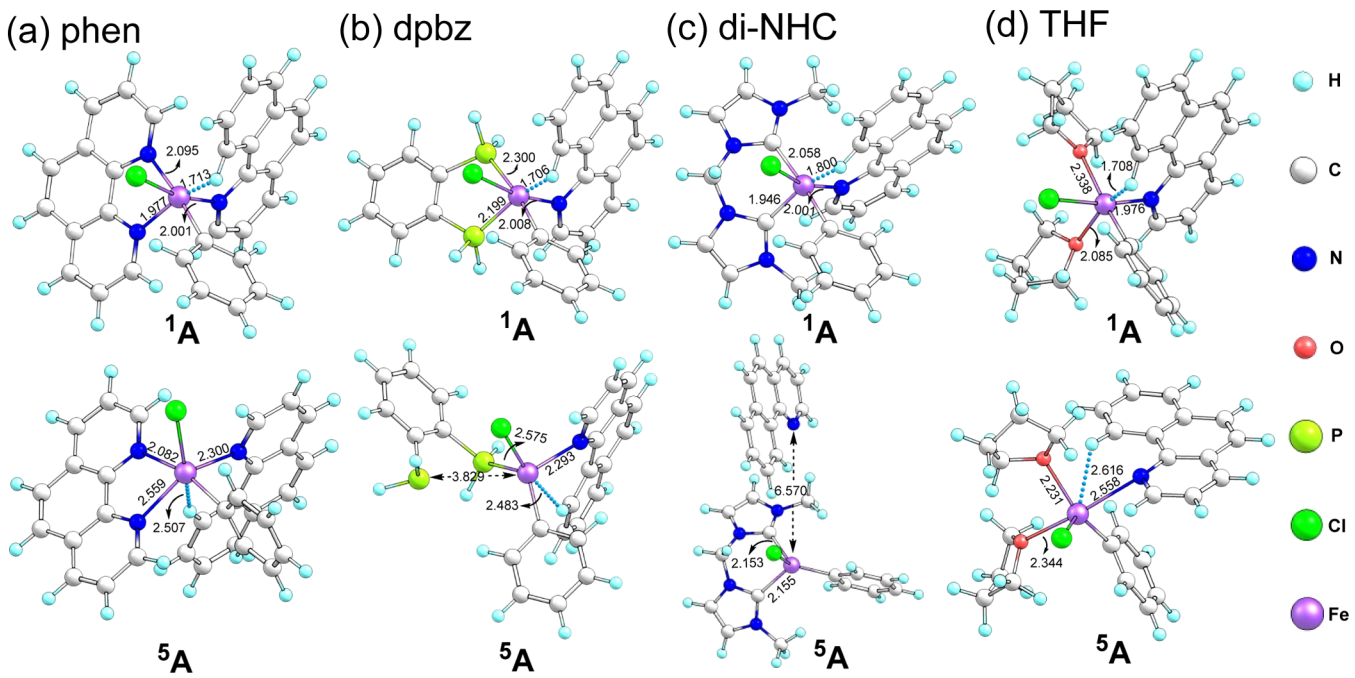


**Figure 11.** Optimized geometries of singlet ($^1$**A**) and quintet ($^5$**A**) RCs [$Fe^{II}$(substrate)(L)(Ph)Cl] (substrate = α-benzoquinoline) for the Fe(II)-mediated $sp^2$ C−H activation step with different ligands (L): (a) phen; (b) dpbz; (c) di-NHC; (d) solvent THF (without specially added ligand).

stabilization of the singlet state compared with phen. However, besides the selective stabilization of the singlet state relative to the quintet state, there is another key but often neglected factor on $\Delta G^{\ddagger}_{eff}$ that makes a difference among ligands. As also noted by Holland,[35a] strong/weak field and strong/weak binding are two different characteristics of ligands that are not necessarily dependent on each other. Specifically, the concept of a strong- or weak-field ligand concerns its ability to split the metal d orbitals, thereby affecting the spin-state gap, while the concept of a strong- or weak-binding ligand has to do with the strength of binding between the ligand and metal, thus controlling the stability of the reactant complexation. As shown in our previous work on C−H activations,[62] the ligand−substrate binding strength is also important for reactivity because it determines the stability and thus the concentration of the C−H activation reactant complex. In the current case, the binding/coordination strength of ligands and substrates in the quintet ground state determines the stability and hence the concentration of the ground-state C−H activation reactant complex $Fe^{II}$(substrate)(L)(Ph)Cl (e.g., $^5$**A** in Figure 10), which thus influences the effectiveness of the C−H activation.

To gauge this aspect of the ligand effect, we used $Fe^{II}(THF)_3(Ph)Cl$ as the common reference for all four differently ligated systems under study and calculated the free energy change for the substrate and ligand binding process in going from $Fe^{II}(THF)_3(Ph)Cl$ to the substrate- and ligand-bound reactant $Fe^{II}$(substrate)(L)(Ph)Cl. This free energy change would faithfully convey the relative binding differences of various ligands plus substrate; the latter could also be influenced by the ligand coordination through interactions


DOI: 10.1021/jacs.5b12150
J. Am. Chem. Soc. 2016, 138, 3715−3730

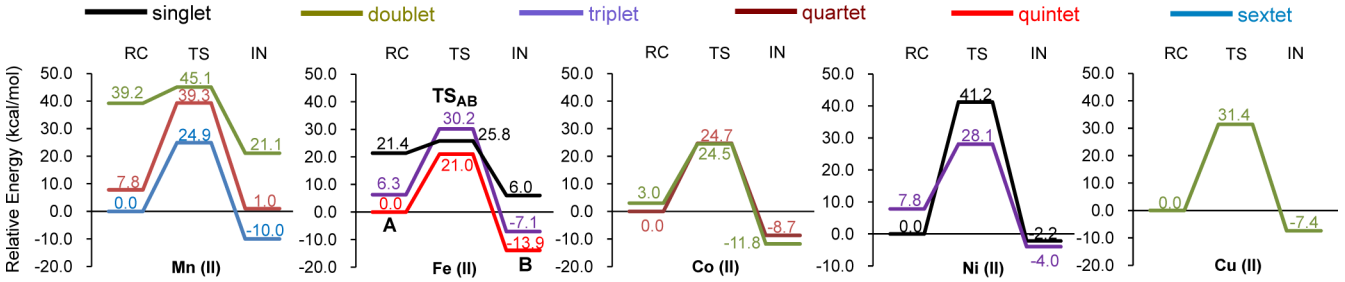


**Figure 12.** Reaction profiles of the $sp^2$ C−H activation step promoted by divalent first-row middle and late TMs (Mn, Fe, Co, Ni, Cu) in the same coordinate environment as from **A** through $\mathbf{TS_{AB}}$ to **B** for the $Fe^{II}$(substrate)(phen)(Ph)Cl complex (substrate = α-benzoquinoline). Relative Gibbs free energies are labeled. All of the calculations were performed in the gas phase rather than in solvent to exhibit the intrinsic properties of the various metals, and no CCSD(T) corrections were used here.

between the ligand and substrate both electronically via the central iron and/or sterically between the ligand and substrate directly. In other words, ligand binding can affect substrate binding, and the free energy change for the binding process computed here covers both of the effects and thereby reveals the relative stability of the C−H activation reactant complex.

Inspecting Figure 10, one finds first that relative to THF as a ligand, the binding strength of ligand plus substrate increases in going from the diphosphine (dpbz) to the dipyridine (phen) and finally to the dicarbene (di-NHC). Thus, dpbz plus substrate ligation is a disfavored endoergic process, while phen plus substrate has slightly exoergic binding and di-NHC plus substrate exhibits the most exoergic bonding. This difference between dpbz and phen is also in line with the experimental fact that when diphosphine ligands were used in low-valent iron-promoted C−H activations, some bidentate directing groups on the substrates were always used to compensate for the weaker ligation of the diphosphine ligand by increasing the substrate binding strength for final stabilization of the reactant complex for C−H activation.[14−18,20,25,26] Interestingly, despite the weaker binding of dpbz compared with phen and di-NHC, as discussed above dpbz can stabilize the singlet-state RC and TS in C−H activation relative to the quintet ground state more than phen does (Figure 10a,b). Hence, if the weaker binding of dpbz plus substrate can be circumvented by some means such as the use of a bidentate directing group, the C−H activation would actually be more efficient than with phen. This phenomenon of enhanced reactivity was also actually observed in experiments when the ligand was changed from phen to dppbz or other diphosphine ligands.[15,26] On the contrary, as shown in Figure 10c, although the dicarbene ligand di-NHC results in much tighter ligand binding than phen and dpbz, it cannot adequately stabilize the singlet state in C−H activation. Hence, this ligand would not be effective in low-valent iron-promoted C−H activation. It should also be noted from Figure 11c that when di-NHC is used, the substrate dissociates from the metal for the reactant complex of the quintet ground state, indicating an unfavorable interaction between the di-NHC ligand and the substrate when they ligate the metal simultaneously.

**3.3. Comparison of Potential C−H Activation by Other First-Row Middle/Late Transition Metals.** Since our theoretical calculations suggest that Fe(II) can promote the C−H activation via TSR, it is of interest to compare the C−H activation reactivities mediated by other divalent middle and late first-row TMs, i.e., Mn(II), Co(II), Ni(II), and Cu(II), in the same coordinate environment as Fe(II) has in the $sp^2$ C−H activation. Similar to Fe(II), all of the possible spin states of these four TMs derived from their d-subshell configurations were considered here. For Mn(II)/Fe(II) with $d^5/d^6$ configurations, this included a maximal number of three spin states, i.e., low-spin (doublet/singlet), medium-spin (quartet/triplet), and high-spin (sextet/quintet), while for Co(II)/Ni(II) with $d^7/d^8$ configurations, the number of spin states was reduced to two, i.e., low-spin (doublet/singlet) and high-spin (quartet/triplet). In the case of Cu(II) with the $d^9$ configuration, only one state (doublet) remains. Comparing the aromatic $sp^2$ C−H activations by Mn(II), Fe(II), Co(II), Ni(II), and Cu(II) (Figure 12), one sees that the two lowest C−H activation barriers, <10 kcal/mol, belong to the low-spin states (singlet/doublet) of the Fe(II) and Mn(II) systems. All of the other spin states or metals have C−H activation barriers of at least 20 kcal/mol. As we already showed, having a low barrier for the low-spin state with an appropriate ligand to stabilize the low-spin state relative to the high-spin ground state leads to efficient Fe(II)-promoted C−H activation. Turning to the Mn(II) system, its inherent advantage of a low C−H activation barrier for the low-spin state is also a promising feature for potential C−H activation reactivity that has not yet been exploited experimentally. As for Fe(II), here too the crucial issue is to find a suitable ligand environment to stabilize the low-spin state sufficiently. This, however, would be a more difficult task than for Fe(II) since Mn(II) has the largest energy penalty for electron pairing among all of the divalent first-row transition metals from its high-spin state, which is strongly exchange-stabilized very stable half-filled d subshell ($d^5$ configuration).[63] This strong exchange stabilization is corroborated by the larger high-spin to low-spin gap for Mn(II) than for Fe(II), as shown in Figure 12. Furthermore, it is noteworthy that the C−H activation barriers on the two spin-state PESs other than the low-spin one are quite large for Mn(II), even larger than those for Fe(II), which implies that without the involvement of low-spin states, Mn(II) will be quite sluggish for the C−H activation process. This implication, along with the known difficulty of stabilizing the low-spin state of Mn(II),[64] may explain why utilizing Mn(II) to activate C−H bonds is still an unmet challenge in experiments. On the basis of the above discussion, further efforts toward ligand design can hopefully resolve this issue.

In contrast to Mn(II) and Fe(II), for Co(II) and Ni(II) the low-spin state has either a similar or even higher C−H activation barrier than the high-spin state, which indicates that the low-spin state for these two divalent TM ions has no advantage in C−H activation reactivity under current ligand environment. For Cu(II), the high barrier of more than 30 kcal/mol for its only available spin state (the doublet state) is


DOI: 10.1021/jacs.5b12150
J. Am. Chem. Soc. 2016, 138, 3715−3730

also an indication that a reaction mode utilizing the phenyl group as the H-atom acceptor should not be an efficient C−H activation pathway for Cu(II). Alternatively, if the acetate group acts as the H-atom acceptor in the Cu(II) case, the barrier can be lowered to about 20 kcal/mol, albeit with a less favorable reaction energy (for details, see Figure S2 in the Supporting Information).

## 4. CONCLUSIONS

In this work, based on DFT and high-level ab initio coupled cluster calculations, we have charted for the first time a detailed reaction mechanism for the puzzling C−H activation reaction promoted by low-valent iron that has recently emerged as one of the promising approaches for C−H activation by earth-abundant first-row transitions metals. Our key mechanistic discoveries for the whole catalytic cycle in the representative C−H arylation reaction include the following:

(a) Fe(II) and Fe(III), possibly present under different experimental conditions, can efficiently promote the C−H activation via a *two-state reactivity (TSR) scenario*, in which the initially excited low-spin singlet and doublet states cross over through the high-spin ground states to promote C−H cleavage. Compared with Fe(II) and Fe(III), Fe(I) and Fe(0) are less energetically favorable to mediate the C−H activation step.

(b) Following C−H activation and aryl transmetalation, Fe(II) undergoes oxidation by the dichloroalkane additive to give Fe(III) through a SET mechanism, which is necessary to effect the final C−C coupling step that completes the C−H functionalization.

(c) For the Fe(I) species generated during the C−C coupling, a mechanism involving SET by the oxidant enables regeneration of the Fe(II) catalyst for the C−H activation in the next round of the catalytic cycle. The alternative pathway, oxidative addition of the dichloroalkane oxidant, is not favored for Fe(I) oxidation compared with the SET pathway.

(d) In total, the reaction mechanisms we have proposed reveal that during the catalytic cycle the iron oxidation states evolve in one of the following sequences: Fe(II)/Fe(III)/Fe(I) or Fe(III)/Fe(I).

In this reaction mechanism, the ligand sphere of iron emerges as a crucial stabilizing factor for the low-spin state and a promoter of C−H activation through TSR. This is the first time that TSR, a productive reactivity concept in the area of high-valent iron chemistry, has been revealed to successfully rationalize the reactivity for a reaction promoted by a low-valent iron system.

A comparative study of the other middle and late first-row transition metals showed that iron is an optimum metal in the current proposed C−H activation mechanism. However, we also suggest that low-spin Mn(II) is another promising candidate for high C−H activation reactivity under adequate low-spin stabilizing circumstances, e.g., enabled by a strong-field ligating environment. This TSR scenario thus constitutes a new strategy for developing C−H activation reactions by low-valent first-row transition metals, the applicability of which awaits more studies in the future.

## ■ ASSOCIATED CONTENT

### Supporting Information

The Supporting Information is available free of charge on the ACS Publications website at DOI: 10.1021/jacs.5b12150.

Two figures showing computational results, absolute energies of all calculated species, T1 diagnostic for the CC calculations, complete refs 36 and 41, and Cartesian coordinates of all calculated species (PDF)

## ■ AUTHOR INFORMATION


### Corresponding Author

*chenh@iccas.ac.cn


### Notes

The authors declare no competing financial interest.

## ■ ACKNOWLEDGMENTS

This work was supported by the National Natural Science Foundation of China (21290194, 21473215, and 21521062). S.S. acknowledges support from the Israel Science Foundation (ISF Grant 1183/13).

## ■ REFERENCES


(1) (a) Yachandra, V. K.; Sauer, K.; Klein, M. P. *Chem. Rev.* **1996**, *96*, 2927−2950. (b) Dismukes, G. C. *Chem. Rev.* **1996**, *96*, 2909−2926. (c) *Manganese Redox Enzymes*; Pecoraro, V. L., Ed.; Wiley-VCH: New York, 1992.

(2) (a) Costas, M.; Mehn, M. P.; Jensen, M. P.; Que, L., Jr. *Chem. Rev.* **2004**, *104*, 939−986. (b) Ortiz de Montellano, P. R. *Chem. Rev.* **2010**, *110*, 932−948. (c) Meunier, B.; de Visser, S. P.; Shaik, S. *Chem. Rev.* **2004**, *104*, 3947−3980. (d) Abu-Omar, M. M.; Loaiza, A.; Hontzeas, N. *Chem. Rev.* **2005**, *105*, 2227−2252. (e) Rosen, G. M.; Tsai, P.; Pou, S. *Chem. Rev.* **2002**, *102*, 1191−1199. (f) Kaila, V. R. I.; Verkhovsky, M. I.; Wikström, M. *Chem. Rev.* **2010**, *110*, 7062−7081. (g) Ferguson-Miller, S.; Babcock, G. T. *Chem. Rev.* **1996**, *96*, 2889−2908. (h) Marletta, M. A.; Hurshman, A. R.; Rusche, K. M. *Curr. Opin. Chem. Biol.* **1998**, *2*, 656−663. (i) Poulos, T. L.; Li, H.; Raman, C. S. *Curr. Opin. Chem. Biol.* **1999**, *3*, 131−137. (j) Groves, J. T.; Wang, C. C.-Y. *Curr. Opin. Chem. Biol.* **2000**, *4*, 687−695. (k) Krebs, C.; Fujimori, D. G.; Walsh, C. T.; Bollinger, J. M., Jr. *Acc. Chem. Res.* **2007**, *40*, 484−492. (l) Kovaleva, E. G.; Neibergall, M. B.; Chakrabarty, S.; Lipscomb, J. D. *Acc. Chem. Res.* **2007**, *40*, 475−483. (m) Wallar, B. J.; Lipscomb, J. D. *Chem. Rev.* **1996**, *96*, 2625−2657. (n) Tinberg, C. E.; Lippard, S. J. *Acc. Chem. Res.* **2011**, *44*, 280−288. (o) Bruijnincx, P. C. A.; van Koten, G.; Klein Gebbink, R. J. M. *Chem. Soc. Rev.* **2008**, *37*, 2716−2744. (p) Solomon, E. I.; Brunold, T. C.; Davis, M. I.; Kemsley, J. N.; Lee, S.-K.; Lehnert, N.; Neese, F.; Skulan, A. J.; Yang, Y.-S.; Zhou, J. *Chem. Rev.* **2000**, *100*, 235−349. (q) Vignais, P. M.; Billoud, B. *Chem. Rev.* **2007**, *107*, 4206−4272. (r) Fontecilla-Camps, J. C.; Volbeda, A.; Cavazza, C.; Nicolet, Y. *Chem. Rev.* **2007**, *107*, 4273−4303. (s) Lubitz, W.; Ogata, H.; Rüdiger, O.; Reijerse, E. *Chem. Rev.* **2014**, *114*, 4081−4148.

(3) (a) Brown, K. L. *Chem. Rev.* **2005**, *105*, 2075−2149. (b) Toraya, T. *Chem. Rev.* **2003**, *103*, 2095−2127. (c) Gruber, K.; Puffer, B.; Kräutler, B. *Chem. Soc. Rev.* **2011**, *40*, 4346−4363.

(4) (a) Can, M.; Armstrong, F. A.; Ragsdale, S. W. *Chem. Rev.* **2014**, *114*, 4149−4174. (b) Maroney, M. J.; Ciurli, S. *Chem. Rev.* **2014**, *114*, 4206−4228. (c) Li, Y.; Zamble, D. B. *Chem. Rev.* **2009**, *109*, 4617−4643.

(5) (a) Solomon, E. I.; Chen, P.; Metz, M.; Lee, S.-K.; Palmer, A. E. *Angew. Chem., Int. Ed.* **2001**, *40*, 4570−4590. (b) Klinman, J. P. *Chem. Rev.* **1996**, *96*, 2541−2561. (c) Solomon, E. I.; Sundaram, U. M.; Machonkin, T. E. *Chem. Rev.* **1996**, *96*, 2563−2606. (d) Balasubramanian, R.; Rosenzweig, A. C. *Acc. Chem. Res.* **2007**, *40*, 573−580. (e) Whittaker, J. W. *Chem. Rev.* **2003**, *103*, 2347−2363.




DOI: 10.1021/jacs.5b12150
*J. Am. Chem. Soc.* 2016, 138, 3715−3730

(6) (a) Lewis, J. C.; Coelho, P. S.; Arnold, F. H. *Chem. Soc. Rev.* **2011**, *40*, 2003−2021. (b) Bollinger, J. M., Jr.; Krebs, C. *Curr. Opin. Chem. Biol.* **2007**, *11*, 151−158. (c) van der Donk, W. A.; Krebs, C.; Bollinger, J. M., Jr. *Curr. Opin. Struct. Biol.* **2010**, *20*, 673−683.
(7) (a) Labinger, J. A.; Bercaw, J. E. *Nature* **2002**, *417*, 507−514. (b) Godula, K.; Sames, D. *Science* **2006**, *312*, 67−72. (c) Arockiam, P. B.; Bruneau, C.; Dixneuf, P. H. *Chem. Rev.* **2012**, *112*, 5879−5918. (d) Lersch, M.; Tilset, M. *Chem. Rev.* **2005**, *105*, 2471−2526. (e) Colby, D. A.; Bergman, R. G.; Ellman, J. A. *Chem. Rev.* **2010**, *110*, 624−655. (f) Lyons, T. W.; Sanford, M. S. *Chem. Rev.* **2010**, *110*, 1147−1169. (g) Ritleng, V.; Sirlin, C.; Pfeffer, M. *Chem. Rev.* **2002**, *102*, 1731−1769. (h) Shilov, A. E.; Shul'pin, G. B. *Chem. Rev.* **1997**, *97*, 2879−2932.
(8) (a) Sun, C.-L.; Li, B.-J.; Shi, Z.-J. *Chem. Rev.* **2011**, *111*, 1293−1314. (b) Su, B.; Cao, Z.-C.; Shi, Z.-J. *Acc. Chem. Res.* **2015**, *48*, 886−896.
(9) Baker, M. V.; Field, L. D. *J. Am. Chem. Soc.* **1987**, *109*, 2825−2826.
(10) Jones, W. D.; Foster, G. P.; Putinas, J. M. *J. Am. Chem. Soc.* **1987**, *109*, 5047−5048.
(11) Waltz, K. M.; He, X.; Muhoro, C.; Hartwig, J. F. *J. Am. Chem. Soc.* **1995**, *117*, 11357−11358.
(12) Klein, H.-F.; Camadanli, S.; Beck, R.; Leukel, D.; Flörke, U. *Angew. Chem., Int. Ed.* **2005**, *44*, 975−977.
(13) Norinder, J.; Matsumoto, A.; Yoshikai, N.; Nakamura, E. *J. Am. Chem. Soc.* **2008**, *130*, 5858−5859.
(14) (a) Asako, S.; Ilies, L.; Nakamura, E. *J. Am. Chem. Soc.* **2013**, *135*, 17755−17757. (b) Cera, G.; Haven, T.; Ackermann, L. *Angew. Chem., Int. Ed.* **2016**, *55*, 1484−1488.
(15) Ilies, L.; Matsubara, T.; Ichikawa, S.; Asako, S.; Nakamura, E. *J. Am. Chem. Soc.* **2014**, *136*, 13126−13129.
(16) Matsubara, T.; Asako, S.; Ilies, L.; Nakamura, E. *J. Am. Chem. Soc.* **2014**, *136*, 646−649.
(17) Monks, B. M.; Fruchey, E. R.; Cook, S. P. *Angew. Chem., Int. Ed.* **2014**, *53*, 11065−11069.
(18) Fruchey, E. R.; Monks, B. M.; Cook, S. P. *J. Am. Chem. Soc.* **2014**, *136*, 13130−13133.
(19) Matsumoto, A.; Ilies, L.; Nakamura, E. *J. Am. Chem. Soc.* **2011**, *133*, 6557−6559.
(20) Ilies, L.; Asako, S.; Nakamura, E. *J. Am. Chem. Soc.* **2011**, *133*, 7672−7675.
(21) Yoshikai, N.; Matsumoto, A.; Norinder, J.; Nakamura, E. *Angew. Chem., Int. Ed.* **2009**, *48*, 2925−2928.
(22) Yoshikai, N.; Asako, S.; Yamakawa, T.; Ilies, L.; Nakamura, E. *Chem. - Asian J.* **2011**, *6*, 3059−3065.
(23) Sirois, J. J.; Davis, R.; DeBoef, B. *Org. Lett.* **2014**, *16*, 868−671.
(24) Shang, R.; Ilies, L.; Asako, S.; Nakamura, E. *J. Am. Chem. Soc.* **2014**, *136*, 14349−14352.
(25) Gu, Q.; Al Mamari, H. H.; Graczyk, K.; Diers, E.; Ackermann, L. *Angew. Chem., Int. Ed.* **2014**, *53*, 3868−3871.
(26) Shang, R.; Ilies, L.; Matsumoto, A.; Nakamura, E. *J. Am. Chem. Soc.* **2013**, *135*, 6030−6032.
(27) Shang, R.; Ilies, L.; Nakamura, E. *J. Am. Chem. Soc.* **2015**, *137*, 7660−7663.
(28) Graczyk, K.; Haven, T.; Ackermann, L. *Chem. - Eur. J.* **2015**, *21*, 8812−8815.
(29) (a) Nam, W. *Acc. Chem. Res.* **2007**, *40*, 522−531. (b) Que, L., Jr. *Acc. Chem. Res.* **2007**, *40*, 493−500. (c) Puri, M.; Que, L., Jr. *Acc. Chem. Res.* **2015**, *48*, 2443−2452. (d) Oloo, W. N.; Que, L., Jr. *Acc. Chem. Res.* **2015**, *48*, 2612−2621. (e) Nam, W. *Acc. Chem. Res.* **2015**, *48*, 2415−2423.
(30) (a) Shaik, S.; Danovich, D.; Fiedler, A.; Schröder, D.; Schwarz, H. *Helv. Chim. Acta* **1995**, *78*, 1393−1407. (b) Shaik, S.; Filatov, M.; Schröder, D.; Schwarz, H. *Chem. - Eur. J.* **1998**, *4*, 193−199. (c) Schröder, D.; Shaik, S.; Schwarz, H. *Acc. Chem. Res.* **2000**, *33*, 139.
(31) (a) Shaik, S.; Hirao, H.; Kumar, D. *Acc. Chem. Res.* **2007**, *40*, 532. (b) Shaik, S.; Kumar, D.; de Visser, S. P.; Altun, A.; Thiel, W. *Chem. Rev.* **2005**, *105*, 2279−2328. (c) Shaik, S.; Cohen, S.; Wang, Y.; Chen, H.; Kumar, D.; Thiel, W. *Chem. Rev.* **2010**, *110*, 949−1017.
(32) (a) Harvey, J. N. *J. Am. Chem. Soc.* **2000**, *122*, 12401−12402. (b) Besora, M.; Carreón-Macedo, J.-L.; Cowan, A. J.; George, M. W.; Harvey, J. N.; Portius, P.; Ronayne, K. L.; Sun, X.-Z.; Towrie, M. *J. Am. Chem. Soc.* **2009**, *131*, 3583−3592. (c) Kalman, S. E.; Petit, A.; Gunnoe, T. B.; Ess, D. H.; Cundari, T. R.; Sabat, M. *Organometallics* **2013**, *32*, 1797−1806. (d) Bellows, S. M.; Cundari, T. R.; Holland, P. L. *Organometallics* **2013**, *32*, 4741−4751. (e) Liu, C.; Cundari, T. R.; Wilson, A. K. *Inorg. Chem.* **2011**, *50*, 8782−8789. (f) Hedström, A.; Lindstedt, E.; Norrby, P.-O. *J. Organomet. Chem.* **2013**, *748*, 51−55.
(33) (a) Maestre, L.; Sameera, W. M. C.; Díaz-Requejo, M. M.; Maseras, F.; Pérez, P. J. *J. Am. Chem. Soc.* **2013**, *135*, 1338−1348. (b) He, R.; Jin, X.; Chen, H.; Huang, Z.-T.; Zheng, Q.-Y.; Wang, C. *J. Am. Chem. Soc.* **2014**, *136*, 6558−6561. (c) Hatakeyama, T.; Hashimoto, S.; Ishizuka, K.; Nakamura, M. *J. Am. Chem. Soc.* **2009**, *131*, 11949−11963.
(34) (a) Poli, R. *Chem. Rev.* **1996**, *96*, 2135−2204. (b) Poli, R. *Acc. Chem. Res.* **1997**, *30*, 494−501. (c) Poli, R.; Harvey, J. N. *Chem. Soc. Rev.* **2003**, *32*, 1−8. (d) Harvey, J. N.; Poli, R.; Smith, K. M. *Coord. Chem. Rev.* **2003**, *238*−*239*, 347−361.
(35) (a) Holland, P. L. *Acc. Chem. Res.* **2015**, *48*, 1696−1702. (b) Power, P. P. *Chem. Rev.* **2012**, *112*, 3482−3507.
(36) Frisch, M. J.; et al. *Gaussian 09*, revision D.01; Gaussian, Inc.: Wallingford, CT, 2009.
(37) (a) Becke, A. D. *Phys. Rev. A: At., Mol., Opt. Phys.* **1988**, *38*, 3098−3100. (b) Lee, C.; Yang, W.; Parr, R. G. *Phys. Rev. B: Condens. Matter Mater. Phys.* **1988**, *37*, 785−789. (c) Becke, A. D. *J. Chem. Phys.* **1993**, *98*, 5648−5652. (d) Becke, A. D. *J. Chem. Phys.* **1993**, *98*, 1372−1377. (e) Stephens, P. J.; Devlin, F. J.; Frisch, M. J.; Chabalowski, C. F. *J. Phys. Chem.* **1994**, *98*, 11623−11627.
(38) Weigend, F.; Ahlrichs, R. *Phys. Chem. Chem. Phys.* **2005**, *7*, 3297−3305.
(39) Marenich, A. V.; Cramer, C. J.; Truhlar, D. G. *J. Phys. Chem. B* **2009**, *113*, 6378−6396.
(40) (a) Grimme, S.; Antony, J.; Ehrlich, S.; Krieg, H. *J. Chem. Phys.* **2010**, *132*, 154104. (b) Grimme, S.; Ehrlich, S.; Goerigk, L. *J. Comput. Chem.* **2011**, *32*, 1456−1465. (c) Becke, A. D.; Johnson, E. R. *J. Chem. Phys.* **2005**, *123*, 154101. (d) Johnson, E. R.; Becke, A. D. *J. Chem. Phys.* **2005**, *123*, 024101. (e) Johnson, E. R.; Becke, A. D. *J. Chem. Phys.* **2006**, *124*, 174104.
(41) Werner, H.-J.; et al. *MOLPRO: A Package of Ab Initio Programs*, version 2010.1; http://www.molpro.net.
(42) (a) Dunning, T. H. *J. Chem. Phys.* **1989**, *90*, 1007−1023. (b) Dunning, T. H.; Peterson, K. A.; Wilson, A. K. *J. Chem. Phys.* **2001**, *114*, 9244−9253. (c) Balabanov, N. B.; Peterson, K. A. *J. Chem. Phys.* **2005**, *123*, 064107.
(43) Martin, J. M. L. *Chem. Phys. Lett.* **1996**, *259*, 669−678.
(44) Feller, D.; Peterson, K. A.; Hill, J. G. *J. Chem. Phys.* **2011**, *135*, 044102.
(45) (a) Chen, H.; Cho, K.-B.; Lai, W. Z.; Nam, W.; Shaik, S. *J. Chem. Theory Comput.* **2012**, *8*, 915−926. (b) Chen, H.; Lai, W. Z.; Shaik, S. *J. Phys. Chem. Lett.* **2010**, *1*, 1533−1540. (c) Oláh, J.; Harvey, J. N. *J. Phys. Chem. A* **2009**, *113*, 7338−7345. (d) Harvey, J. N.; Aschi, M. *Faraday Discuss.* **2003**, *124*, 129−143. (e) Villaume, S.; Daniel, C.; Strich, A.; Perera, S. A.; Bartlett, R. J. *J. Chem. Phys.* **2005**, *122*, 044313. (f) Carreón-Macedo, J.-L.; Harvey, J. N. *Phys. Chem. Chem. Phys.* **2006**, *8*, 93−100.
(46) Bedford, R. B. *Acc. Chem. Res.* **2015**, *48*, 1485−1493.
(47) Nakamura, E.; Yoshikai, N. *J. Org. Chem.* **2010**, *75*, 6061−6067.
(48) (a) Reiher, M.; Salomon, O.; Hess, B. A. *Theor. Chem. Acc.* **2001**, *107*, 48−55. (b) Paulsen, H.; Duelund, L.; Winkler, H.; Toftlund, H.; Trautwein, A. X. *Inorg. Chem.* **2001**, *40*, 2201−2203. (c) Harvey, J. N. *Struct. Bonding (Berlin, Ger.)* **2004**, *112*, 151−183. (d) Swart, M.; Groenhof, A. R.; Ehlers, A. W.; Lammertsma, K. *J. Phys. Chem. A* **2004**, *108*, 5479−5483. (e) Strickland, N.; Harvey, J. N. *J. Phys. Chem. B* **2007**, *111*, 841−852. (f) Conradie, J.; Ghosh, A. *J. Phys. Chem. B* **2007**, *111*, 12621−12624. (g) Liao, M.-S.; Watts, J. D.; Huang, M.-J. *J. Phys. Chem. A* **2007**, *111*, 5927−5935. (h) Zein, S.; Borshch, S. A.; Fleurat-Lessard, P.; Casida, M. E.; Chermette, H. *J. Chem. Phys.* **2007**, *126*, 014105. (i) Fouqueau, A.; Mer, S.; Casida, M.


DOI: 10.1021/jacs.5b12150
J. Am. Chem. Soc. 2016, 138, 3715−3730

E.; Lawson Daku, L. M.; Hauser, A.; Mineva, T.; Neese, F. *J. Chem. Phys.* **2004**, *120*, 9473−9486. (j) Fouqueau, A.; Casida, M. E.; Daku, L. M. L.; Hauser, A.; Neese, F. *J. Chem. Phys.* **2005**, *122*, 044110. (k) Pierloot, K.; Vancoillie, S. *J. Chem. Phys.* **2006**, *125*, 124303. (l) Pierloot, K.; Vancoillie, S. *J. Chem. Phys.* **2008**, *128*, 034104. (m) Radoń, M.; Pierloot, K. *J. Phys. Chem. A* **2008**, *112*, 11824−11832. (n) Radoń, M.; Broclawik, E.; Pierloot, K. *J. Phys. Chem. B* **2010**, *114*, 1518−1528. (o) Chen, H.; Lai, W. Z.; Shaik, S. *J. Phys. Chem. B* **2011**, *115*, 1727−1742.

(49) (a) Watson, P. L.; Parshall, G. W. *Acc. Chem. Res.* **1985**, *18*, 51−56. (b) Vastine, B. A.; Hall, M. B. *Coord. Chem. Rev.* **2009**, *253*, 1202−1218. (c) Lin, Z. *Coord. Chem. Rev.* **2007**, *251*, 2280−2291.

(50) (a) Bryndza, H. E.; Fong, L. K.; Paciello, R. A.; Tam, W.; Bercaw, J. E. *J. Am. Chem. Soc.* **1987**, *109*, 1444−1456. (b) Schock, L. E.; Marks, T. J. *J. Am. Chem. Soc.* **1988**, *110*, 7701−7715. (c) Holland, P. L.; Andersen, R. A.; Bergman, R. G.; Huang, J. K.; Nolan, S. P. *J. Am. Chem. Soc.* **1997**, *119*, 12800−12814. (d) Jones, W. D.; Hessell, E. T. *J. Am. Chem. Soc.* **1993**, *115*, 554−562. (e) Bennett, J. L.; Wolczanski, P. T. *J. Am. Chem. Soc.* **1997**, *119*, 10696−10719.

(51) (a) Clot, E.; Besora, M.; Maseras, F.; Mégret, C.; Eisenstein, O.; Oelckers, B.; Perutz, R. N. *Chem. Commun.* **2003**, 490−491. (b) Clot, E.; Mégret, C.; Eisenstein, O.; Perutz, R. N. *J. Am. Chem. Soc.* **2006**, *128*, 8350−8357. (c) Clot, E.; Mégret, C.; Eisenstein, O.; Perutz, R. N. *J. Am. Chem. Soc.* **2009**, *131*, 7817−7827. (d) Chatwin, S. L.; Davidson, M. G.; Doherty, C.; Donald, S. M.; Jazzar, R. F. R.; Macgregor, S. A.; McIntyre, G. J.; Mahon, M. F.; Whittlesey. *Organometallics* **2006**, *25*, 99−110. (e) Mitoraj, M.; Zhu, H.; Michalak, A.; Ziegler, T. *Organometallics* **2007**, *26*, 1627−1634. (f) Diggle, R. A.; Kennedy, A. A.; Macgregor, S. A.; Whittlesey, M. K. *Organometallics* **2008**, *27*, 938−944. (g) Evans, M. E.; Burke, C. L.; Yaibuathes, S.; Clot, E.; Eisenstein, O.; Jones, W. D. *J. Am. Chem. Soc.* **2009**, *131*, 13464−13473. (h) Choi, G.; Morris, J.; Brennessel, W. W.; Jones, W. D. *J. Am. Chem. Soc.* **2012**, *134*, 9276−9284. (i) Jiao, Y.; Evans, M. E.; Morris, J.; Brennessel, W. W.; Jones, W. D. *J. Am. Chem. Soc.* **2013**, *135*, 6994−7004. (j) Jiao, Y.; Morris, J.; Brennessel, W. W.; Jones, W. D. *J. Am. Chem. Soc.* **2013**, *135*, 16198−16212. (k) Lu, Q.; Yu, H.; Fu, Y. *Chem. Commun.* **2013**, *49*, 10847−10849.

(52) (a) Armentrout, P. B.; Beauchamp, J. L. *Acc. Chem. Res.* **1989**, *22*, 315−321. (b) Li, Z.-Y.; Hu, L.; Liu, Q.-Y.; Ning, C.-G.; Chen, H.; He, S.-G.; Yao, J. *Chem. - Eur. J.* **2015**, *21*, 17748−17756.

(53) (a) Bedford, R. B.; Carter, E.; Cogswell, P. M.; Gower, N. J.; Haddow, M. F.; Harvey, J. N.; Murphy, D. M.; Neeve, E. C.; Nunn, J. *Angew. Chem., Int. Ed.* **2013**, *52*, 1285−1288. (b) Bedford, R. B.; Brenner, P. B.; Carter, E.; Clifton, J.; Cogswell, P. M.; Gower, N. J.; Haddow, M. F.; Harvey, J. N.; Kehl, J. A.; Murphy, D. M.; Neeve, E. C.; Neidig, M. L.; Nunn, J.; Snyder, B. E. R.; Taylor, J. *Organometallics* **2014**, *33*, 5767−5780. (c) Bedford, R. B.; Brenner, P. B.; Carter, E.; Gallagher, T.; Murphy, D. M.; Pye, D. R. *Organometallics* **2014**, *33*, 5940−5943. (d) Adams, C. J.; Bedford, R. B.; Carter, E.; Gower, N. J.; Haddow, M. F.; Harvey, J. N.; Huwe, M.; Cartes, M. A.; Mansell, S. M.; Mendoza, C.; Murphy, D. M.; Neeve, E. C.; Nunn, J. *J. Am. Chem. Soc.* **2012**, *134*, 10333−10336.

(54) (a) Chirik, P. J.; Wieghardt, K. *Science* **2010**, *327*, 794−795. (b) Chirik, P. J. *Acc. Chem. Res.* **2015**, *48*, 1687−1695. (c) Suarez, A. I. O.; Lyaskovskyy, V.; Reek, J. N. H.; van der Vlugt, J. I.; de Bruin, B. *Angew. Chem., Int. Ed.* **2013**, *52*, 12510−12529. (d) Blanchard, S.; Derat, E.; Desage-El Murr, M.; Fensterbank, L.; Malacria, M.; Mouriès-Mansuy, V. *Eur. J. Inorg. Chem.* **2012**, *2012*, 376−389. (e) Luca, O. R.; Crabtree, R. H. *Chem. Soc. Rev.* **2013**, *42*, 1440−1459. (f) Praneeth, V. K. K.; Ringenberg, M. R.; Ward, T. R. *Angew. Chem., Int. Ed.* **2012**, *51*, 10228−10234. (g) Broere, D. L. J.; Plessius, R.; van der Vlugt, J. I. *Chem. Soc. Rev.* **2015**, *44*, 6886−6915.

(55) For recent reviews of C−H activation by low-valent cobalt, see: (a) Gao, K.; Yoshikai, N. *Acc. Chem. Res.* **2014**, *47*, 1208−1219. (b) Moselage, M.; Li, J.; Ackermann, L. *ACS Catal.* **2016**, *6*, 498−525.

(56) For a recent theoretical work on C−H activation by Co(0) via an oxidative addition mechanism, see: Yang, Z.; Yu, H.; Fu, Y. *Chem. - Eur. J.* **2013**, *19*, 12093−12103.

(57) Fallon, B. J.; Derat, E.; Amatore, M.; Aubert, C.; Chemla, F.; Ferreira, F.; Perez-Luna, A.; Petit, M. *J. Am. Chem. Soc.* **2015**, *137*, 2448−2451.

(58) Lau, W.; Huffman, J. C.; Kochi, J. K. *Organometallics* **1982**, *1*, 155−169.

(59) (a) Liu, Y.; Xiao, J.; Wang, L.; Song, Y.; Deng, L. *Organometallics* **2015**, *34*, 599−605. (b) Liu, Y.; Wang, L.; Deng, L. *Organometallics* **2015**, *34*, 4401−4407. (c) Wang, X.; Zhang, J.; Wang, L.; Deng, L. *Organometallics* **2015**, *34*, 2775−2782.

(60) (a) Nakamura, M.; Matsuo, K.; Ito, S.; Nakamura, E. *J. Am. Chem. Soc.* **2004**, *126*, 3686−3687. (b) Noda, D.; Sunada, Y.; Hatakeyama, T.; Nakamura, M.; Nagashima, H. *J. Am. Chem. Soc.* **2009**, *131*, 6078−6079. (c) Daifuku, S. L.; Al-Afyouni, M. H.; Snyder, B. E. R.; Kneebone, J. L.; Neidig, M. L. *J. Am. Chem. Soc.* **2014**, *136*, 9132−9143. (d) Sun, C.-L.; Krause, H.; Fürstner, A. *Adv. Synth. Catal.* **2014**, *356*, 1281−1291.

(61) Hoyt, J. M.; Schmidt, V. A.; Tondreau, A. M.; Chirik, P. J. *Science* **2015**, *349*, 960−963.

(62) (a) Tang, H.; Zhou, B.; Huang, X.-R.; Wang, C.; Yao, J.; Chen, H. *ACS Catal.* **2014**, *4*, 649−656. (b) Tang, H.; Huang, X.-R.; Yao, J.; Chen, H. *J. Org. Chem.* **2015**, *80*, 4672−4682.

(63) Lever, A. B. P. *Inorganic Electronic Spectroscopy*, 2nd ed.; Elsevier: New York, 1984; p 750.

(64) (a) Ganguly, S.; Karmakar, S.; Pal, C. K.; Chakravorty, A. *Inorg. Chem.* **1999**, *38*, 5984−5987. (b) Karmakar, S.; Choudhury, S. B.; Chakravorty, A. *Inorg. Chem.* **1994**, *33*, 6148−6153. (c) Saha, A.; Majumdar, P.; Goswami, S. *J. Chem. Soc., Dalton Trans.* **2000**, 1703−1708 and references therein.



DOI: 10.1021/jacs.5b12150
*J. Am. Chem. Soc.* 2016, 138, 3715−3730